CZECH TECHNICAL UNIVERSITY IN PRAGUE
FACULTY OF BIOMEDICAL ENGINEERING
Department of Natural Sciences

Characterization of size of polydisperse nanoparticles of various shape: Comparative study of AFM and DLS methods

Master Thesis

Study programme: Biomedical and Clinical Technology
Study branch: Instruments and Methods for Biomedicine

Supervisor: Ing. Vladimíra Petráková, Ph.D.

Bc. Andrea Mineva

Kladno 2017

České vysoké učení technické v Praze, Fakulta biomedicínského inženýrství

Katedra přírodovědných oborů

Akademický rok: 2016/2017

Zadání diplomové práce

Student: **Bc. Andrea Mineva**

Studijní obor: Přístroje a metody pro biomedicínu

Téma: **Charakterizace velikosti polydisperzních nanočástic rozličných tvarů: Komparativní studie metod AFM a DLS**

Téma anglicky: Characterization of size of polydispers nanoparticles of various shape: Comparative study of AFM and DLS methods

Zásady pro vypracování:

Vlastnosti nanočástic a jejich další aplikace v biomedicíně závisí na jejich velikosti a tvaru. Při přípravě a syntéze nanočástic různých tvarů je nutné mít metodu, která poskytne s požadovanou přesností zpětnou vazbu o charakteristikách materiálu. Mezi tyto charakteristiky nejčastěji patří velikost, poměr stran a rozložení velikostních frakcí v případě polydisperzních nanočástic.
Cílem této práce je porovnat metody, které se využívají k charakterizaci velikosti nanočástic a diskutovat jejich vhodnost pro měření nanočástice rozmanitých tvarů, velikostí a stupně polydisperzity.

1) Seznamte se s principy metod využívaných k charakterizaci velikosti nanočástic: Dynamický rozptyl světla (DLS), Mikroskopie atomárních sil (AFM), Elektronová mikroskopie (SEM)
2) Na referenčních vzorcích optimalizujte podmínky měření metodou AFM v různých podmínkách (voda/vzduch)
3) Optimalizujte depozici nanočástic na podložku pro měření AFM tak, aby se minimalizovala agregace nanočástic
4) Vytvořte program na zpracování obrazových dat z měření AFM
5) Metodou DLS a AFM charakterizujte vzorky zlatých nanočástic a zlatých nanotyčinek (nanorods) o různých poměrech stran a různého stupně tvarové homogenity
6) Porovnejte výsledky velikostní analýzy a diskutujte parametry (velikost, tvar, polydisperzita), které mají největší vliv na přesnost měření jednotlivými metodami. Jako referenci použijte obrázky z elektronového mikroskopu (SEM)

Seznam odborné literatury:

[1] Hoo, C.M., Starostin, N., West, P. et al. , A comparison of atomic force microscopy (AFM) and dynamic light scattering (DLS) methods to characterize nanoparticle size distributions, Journal of Nanoparticle Research, Vol. 10, No. 89, 2008
[2] Rehor, I, Cigler, P, Precise estimation of HPHT nanodiamond size distribution based on transmission electron microscopy image analysis, Diamond and related materials, Vol. 46, No. 21, 2014, 10.1016/j.diamond.2014.04.002

Vedoucí: Ing. Vladimíra Petráková, Ph.D.

Zadání platné do: 20.08.2018

.....
vedoucí katedry / pracoviště

.....
děkan

V Kladně dne 05.01.2017

Czech Technical University in Prague, Faculty of Biomedical Engineering

Academic year: 2016/2017

Diploma thesis assignment

(Master project thesis assignment)

Student:	**Bc. Andrea Mineva**
Study branch:	Instruments and Methods for Biomedicine
Title:	**Characterization of size of polydispers nanoparticles of various shape: Comparative study of AFM and DLS methods**
Title in Czech:	Charakterizace velikosti polydisperzních nanočástic rozličných tvarů: Komparativní studie metod AFM a DLS

Instructions for processing:

Nanoparticle properties and their applications are given by their size and shape. During the preparation and synthesis of nanoparticles of various shapes there is a need of having a method, which offers a feedback with the desired precision about the material characteristics. Among these characteristics are most often size, aspect ratio and fraction distribution in the case of polydisperse nanoparticles.
The aim of this work is to compare methods used for nanoparticle size characterization and to discuss their applicability for measurements of nanoparticles of different shapes, sizes and polydispersity.

1) Become acquainted with the principles of methods used for nanoparticles size characterization: Dynamic Light Scattering (DLS), Atomic Force Microscopy (AFM), Scanning Electron microscopy (SEM).
2) Optimize the conditions for measurements using AFM in different mediums (water/air) using reference samples.
3) Optimize the deposition of nanoparticles on the substrate for AFM measurements to minimize nanoparticle aggregation.
4) Write a program for image analysis of the data from AFM measurements.
5) Characterize samples of gold nanoparticles and nanorods of different aspect ratios and different degrees of shape homogeneity using DLS and AFM methods.
6) Compare the results of the size analysis and discuss the parameters (size, shape, polydispersity) that have the biggest effect on measurement accuracy using the different methods. As reference use the images obtained from a Scanning Electron Microscope (SEM).

References:

[1] Hoo, C.M., Starostin, N., West, P. et al. , A comparison of atomic force microscopy (AFM) and dynamic light scattering (DLS) methods to characterize nanoparticle size distributions, Journal of Nanoparticle Research, Vol. 10, No. 89, 2008
[2] Rehor, I, Cigler, P, Precise estimation of HPHT nanodiamond size distribution based on transmission electron microscopy image analysis, Diamond and related materials, Vol. 46, No. 21, 2014, 10.1016/j.diamond.2014.04.002

Validity of assignment until date: 20.08.2018

Supervisor of diploma thesis: Ing. Vladimíra Petráková, Ph.D.

....

Head of Department Dean

In Kladno, 06.03.2017

PROHLÁŠENÍ

Prohlašuji, že jsem diplomovou práci s názvem Charakterizace velikosti polydisperzních nanočástic rozličných tvarů: Komparativní studie metod AFM a DLS vypracovala samostatně a použila k tomu úplný výčet citací použitých pramenů, které uvádím v seznamu přiloženém k diplomové práci.

Nemám závažný důvod proti užití tohoto školního díla ve smyslu § 60 zákona č. 121/2000 Sb., o právu autorském, o právech souvisejících s právem autorským a o změně některých zákonů (autorský zákon), ve znění pozdějších předpisů.

V Kladně dne …… ……..

Bc. Andrea Mineva

ACKNOWLEDGEMENTS

On the first place I would like to thank my supervisor Ing. Vladimíra Petráková, Ph.D. for her patience and tolerance during the whole work. Also for her mental encouragement. Secondly I would like to acknowledge the assistance of Ing. Martin Otáhal, for his kind help with whatever came to my mind. Also, I would like to thank Ing. Marek Kindermann for his great help with everything regarding the DLS method.

And last, but not least, I would really like to thank my whole family, my mother, father, brother and partner, because of their support, love and quiet tolerance, even during hard times.

NÁZEV DIPLOMOVÉ PRÁCE:

Charakterizace velikosti polydisperzních nanočástic rozličných tvarů: Komparativní studie metod AFM a DLS

ABSTRAKT:

Běžné materiály získávají nové vlastnosti, ať již optické, fyzikální, chemické a jiné, jsou-li vyrobeny v nanorozměrech. Tato skutečnost je převážně spojena s faktem, že takto male částice mají velký poměr plochy ku objemu v porovnání s běžnými konfiguracemi těchto materiálů. Vlastnosti nanočástic závisí z převážné části na jejich velikosti a tvaru. Proto je důležité mít prostředek pro určování velikosti a tvaru, s touto znalostí by pak bylo možné i předpovídat vlastnosti dodaných nanočástic. Kovové nanočástice jsou skvělým modelovým materiálem díky své snadné syntéze v různých velikostech a tvarech. Existuje mnoho metod pro určování velikostní distribuce nanočástic. Cílem této práce je použití dvou různých metod – mikroskopu atomárních sil (AFM) a dynamického rozptylu světla (DLS) – jejich porovnání a diskuze jejich vhodnosti pro charakterizaci tvaru a velikosti nanočástic. Kovové nanočástice byly deponovány na sklíčko pro AFM měření, pro měření pomocí DLS zůstaly v koloidním roztoku. Byl napsán program pro zpracování obrazových dat z výsledků AFM. Získaná data byla porovnána s výsledky Transmisního elektronového mikroskopu (TEM). Výsledky ukazují, že AFM i DLS měření vedou k srovnatelných výsledkům, v případě sférických nanočástic. Nicméně, DLS není možno, v daném nastavení, použít pro charakterizaci nanočástic ve tvaru tyčí. Oproti tomu AFM je, i přes komplikovanější analýzu dat, srovnatelné s TEM.

KLÍČOVÁ SLOVA:

Zlaté nanočástice, Velikost nanočástic, AFM, DLS

MASTER THESIS TITLE:

Characterization of size of polydisperse nanoparticles of various shape: Comparative study of AFM and DLS methods

ABSTRACT:

When produced in nanometre sizes, ordinary materials obtain new and exciting properties – optical, physical, chemical and others. This is mainly connected to the fact that such small particles offer a great surface-to-volume ratio, unlike bulk materials. These properties and characteristics are greatly dependent on the nanoparticle size and shape. Therefore, it is important to have a tool of determining the nanoparticle size and shape in order to predict its behaviour when using them. Metallic nanoparticles are a great material for a model system, because of their easy synthesis in different sizes and shapes. There are multiple methods for nanoparticle size distribution determination. The aim of this study is to use two of these methods – Atomic Force Microscopy (AFM) and Dynamic Light Scattering (DLS) – compare them and discuss their suitability for characterizing nanoparticle size and shape for samples of different shapes. The metallic nanoparticle (gold and silver) samples were prepared for AFM by deposition on a cover glass, for DLS they remained in a colloidal solution. An image processing program was programmed for the data analysis of AFM results. The data were compared to TEM images. Our results show that the AFM and DLS methods are quite comparable in the means of spherical nanoparticles, however DLS in the setup used cannot characterize rod-like nanoparticles, whereas AFM in such cases is, even with difficult data analysis, comparable to the TEM images.

KEY WORDS:

Gold nanoparticles, Size distribution, AFM, DLS,

CONTENT

ABBREVIATIONS

AR – aspect ratio

AuNP – gold nanoparticles

AuNR – gold nanorods

AgNP – silver nanoparticles

SPR – surface plasmon resonance

PTT – photothermal therapy

PPTT – plasmon photothermal therapy

AFM – atomic force microscopy

FS – force spectroscopy

DLS – dynamic light scattering

TEM – transmission electron microscopy

SEM – scanning electron microscopy

Rcf – relative centrifugal force

ANUC – analytical ultracentrifugation

CTAB – Cetrimonium bromide

1. INTRODUCTION

Nanoparticles are a novel and innovative material, which derives its unique optical, physical, biological and other properties form its size, more precisely surface/volume ratio, which distinguishes nanoparticles from their bulk counterparts. This allows an innovative approach to numerous fields, as nanoparticles are utilizable as useful tools in not only biomedicine but also in material sciences, industry and others. Nanoparticle properties vary in dependence of the material used and thus a suitable nanoparticle can be found for the desired function. Gold (AuNP) and silver (AgNP) nanoparticles are ones that are frequently used in biomedical fields, where they can be applied as diagnostic agents or therapeutic mediators. Moreover, their accessible synthesis in different shapes and sizes makes metallic nanoparticles – gold and silver – a suitable material for a model system.

The properties of nanoparticles that are so greatly utilized in biomedicine, such as optical and physical properties or toxicity, vary greatly in dependence on the size and the shape of the particles. Therefore, it is important to characterize the particle shape and size distribution in order to correctly understand (and even predict) the properties.

There are multiple methods for characterizing particle size distribution. Microscopic methods are the most often used ones, especially Scanning Electron Microscopy (SEM) or Transmission Electron Microscopy (TEM). A relatively newer method is that of Atomic Force Microscopy (AFM), which offers down to atomic resolution and is therefore more than suitable for nanoparticle size and shape determination. Dynamic Light Scattering (DLS) is a non-microscopic method, which is also commonly used as a size determination tool based on evaluation of particle motion through changes in the light they scatter. DLS is therefore an indirect method of size determination.

The main practical differences between microscopy methods and DLS are the speed of analysis and the precision of size evaluation. While DLS is a “plug-in” fast method that measures the sample as a whole, AFM image is reconstructed point-by point by probe moving across the sample and one image can take up to hours and measures on a single particle level. In general, DLS is considered more practical for fast analysis of nanoparticle size and AFM as a time consuming but very precise method.

AFM and DLS have been previously compared in connection with nanoparticle size distribution, however different shapes of nanoparticles introduce a new perspective to this problem.

The main aim of this study is to compare the AFM and DLS methods for nanoparticle size distribution characterization on gold and silver nanoparticles and discuss the suitability of these methods for characterization of the shape and size of nanoparticles in mono- and poly-disperse samples. And to tackle the strengths and weaknesses of these methods in the challenge of characterization of size and shape of nanoparticles in liquid environment. First, the measurements using AFM were optimized while measuring a reference sample using different modes. For the AFM measurements, the deposition of AuNP on glass was optimized to avoid particle aggregation and for the data analysis of the AFM measurements a program in MATLAB was written.

This work is divided into five parts. First, the theoretical background for the problem is presented, including AuNP and AgNP characteristics and present methods used in particle size determination. The second part focuses on the state of the art and describes the size characterization of different nanoparticles in multiple studies. In the third part of this work, *Equipment and Methods*, the equipment and methods used in the work are described. The results are presented in the fourth part. Finally, the results as well as the methods used are discussed and compared to literature.

2. THEORY

The theoretical background of the nanoparticles and the methods that can be used in nanoparticle size determination is discussed in the following section.

2.1. NANOPARTICLES

Nano is a prefix used to describe a 10^{-9}, or one billionth of a quantity. The use of nano as a word is mainly to describe nanoparticles, elements in the size of ones to hundreds of nanometres (billionths of a meter). [1]

When produced as nanoparticles, ordinary materials obtain new and exciting properties and characteristics, opening new possibilities for use. These properties are mainly connected to the fact that unlike with bulk materials, nanoparticles offer a great surface/volume ratio. With bulk materials, the surface size is neglectable in comparison to the volume, whereas nanoparticles have a large surface area. If we compare the same volume of a bulk material and nanoparticles, the overall surface of nanoparticles is several times greater (Figure 2.1). This alters the chemical reactivity of nanoparticles. Bulk materials, which are normally inert, increase their reactivity when produced as nanoparticles. [1] [2]

As the nanoparticle size increases, the surface to volume ratio decreases, which changes the nanoparticle properties. Thus, the nanoparticle properties greatly depend on the size. [1]

Plenty of biological mechanisms also occur at the nanoscale. Elements inside of cells often have a size of ones of nanometres. For example, a strand of DNA has a diameter of about 2 nm. Haemoglobin, the transport protein carrying oxygen and carbon dioxide through the body, has a dimeter of about 5 nm. The fact that nanoparticles have about the same size as proteins makes them a material suitable for biolabeling and imaging. [2] [3] [4]

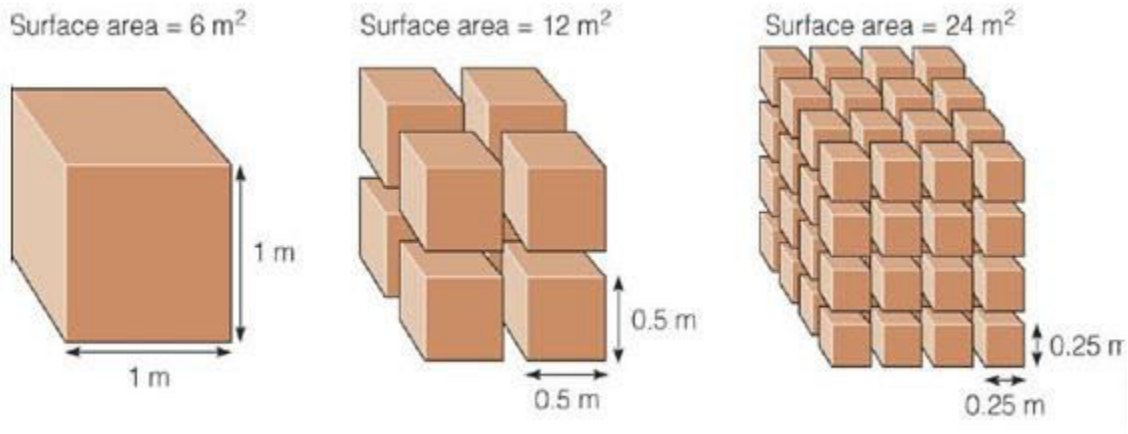

Figure 2.1: *A depiction of the increase of surface to volume ratio when the size of the particle is decreased. Left is a bulk cube of a given volume, with a surface area of 6 m2, a cube of the same volume, consisting of 8 or 64 cubes has an increased surface area, therefore an increased surface/volume ratio. Picture from https://ninithi.files.wordpress.com/2015/06/area.jpg.*

Due to their small size, when compared to cells, nanoparticles can be used as probes to inspect cellular processes inside the cells without interfering with the biological structures too much. There are several factors that influence the nanoparticle cell interactions (Figure 2.2). Apart from particle functionalization – ligand density, the properties of the cell – receptor expression levels, the mechanism of internalization, phenotype, location, also the size, shape and charge of the nanoparticles plays an important role. [3] [5]

The particle shape greatly influences the uptake by the cell – nanorods being the most effective (with nanorods of shorter aspect ratios experiencing increased uptake) in comparison with spheres (bigger than 100 nm), cylinders and cubes (in order of uptake efficiency). Spheres with sizes bellow 100 nm show an increase in uptake even to values above those for nanorods. The location of the ligands affect the binding and subsequent uptake as well. [6] [7] [8]

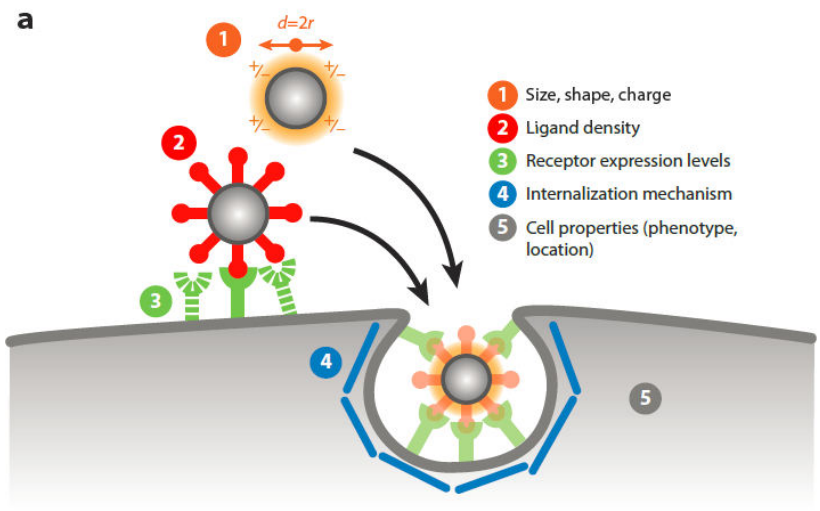

***Figure 2.2**: Properties affecting the nanoparticle cell interaction. They can be either properties of the nanoparticle (size, shape, charge) or of the biological elements involved in the process, as well as the cell properties. Picture from [3].*

The dependence of nanoparticle uptake by the cell on the size is speculated to be due to the membrane wrapping process. The smaller the nanoparticle, the less receptors it binds to, the uptake is therefore smaller because the energy to drive membrane wrapping is not sufficient. Several nanoparticles of such small sizes (ones of nanometres) must bind close together to drive the uptake. On the other hand, too big nanoparticles (above 50 nm) bind to a large number of receptors, which leads to redistribution of receptors on the membrane to compensate for the local depletion. This again leads to decrease in membrane uptake. However, the cells involved are a crucial part of the whole process, the size dependency varies with different cell lines. [9] [10]

Nanoparticles show a great perspective as materials for diagnostics and therapy. This includes their use *in vivo*, which means that there is a need to understand, what happens with the particles within the body, mostly after it achieved the desired effect. The fate of the nanoparticles depends on size, shape and surface chemistry as well. This can be shown on the circulation lifetime (the time, between particle administration to the blood and its uptake by phagocytic cells) of different particles, nanorods (rod shaped micelles) have about ten times longer circulation lifetime than nanospheres. [11] [12] One of the biggest concern is the elimination of nanoparticles from the body. Here, size is an important factor, small particles below 6 nm can be eliminated by the kidney. [13] Larger nanoparticles stay in the body and accumulate in

the spleen and liver. This is of great concern because of the potential toxicity these non-eliminated nanoparticles can cause. [14] Another biological barrier for the nanoparticles is the hematoencephalic barrier, where the upper limit is 5 – 50 nm. [15]

All of these information lead to the fact that the size and shape of nanoparticles are crucial properties influencing not only their other physical characteristics but also their interactions with other (living) systems. Therefore, there is a great need for methods capable of sufficiently determining the size and shape. This would provide a feedback during nanoparticle synthesis as well as enable the prediction of nanoparticle behaviour within certain systems, such as cell cultures or even the whole body.

2.2. METALLIC NANOPARTICLES

In this work, metallic nanoparticles – gold (AuNP) and silver (AgNP) – were used. These nanoparticles are a great model system, because of their easy synthesis in different shapes and sizes. They are also used in the biomedical field, which adds another justification for their use. This chapter describes AuNP and AgNP in general, their properties and applications.

Metallic nanoparticles (more specifically AuNP) have been used for centuries (unknowingly) by artists due to their unique optical properties for glass dying. [16] Depending on the shape, size and environment, the scattered light off AuNP changes its wavelength (Figure 2.3). This is caused by the so called Surface Plasmon Resonance (SPR) effect, observable in all metallic nanoparticles. SPR is an oscillation of the free electrons in the nanoparticles conduction band, which oscillate in resonance with the incident light frequency. [17] [18] Two decay mechanisms exist, either a radiative (where the result is scattering of the light) or nonradiative (where the photon energy is transformed into thermal energy). [19] Both effects can be utilized in biomedicine as well, either in molecule imaging (radiative decay) [20] or in therapy (nonradiative decay). The use of AuNP in Photothermal Therapy (PTT) is referred to as Plasmonic Photothermal Therapy (PPTT) [21] [22]. Colloidal gold has been widely used with different microscopy techniques, such as Confocal Microscopy, in medical and biological research. [23]

Depending on the preparation technique, the nanoparticle surface can be functionalized using different surface groups. Drug delivery agents is thus one of the functions metallic nanoparticles

can provide. This can be done either by adsorption of the drug directly onto the nanoparticle, or by using linkers. [24] [25]

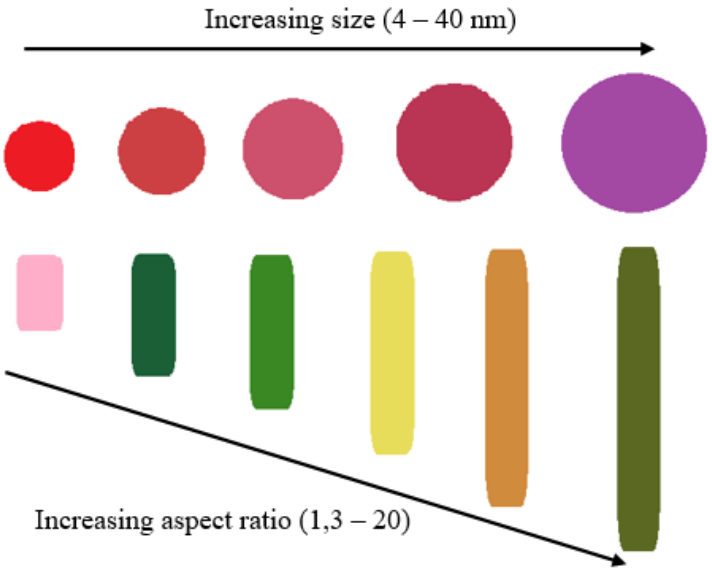

***Figure 2.3**: Effects of particle size and shape on the optical properties. Here, AuNP spheres of increasing size depicted in the colour they express and AuNP rods of increasing aspect ratio depicted the same way. Picture inspired by https://ninithi.files.wordpress.com/2015/07/shape.jpg.*

With nanorods (NRs) the properties change a little, and are, as with spherical nanoparticles, dependent on the size and shape of the particle. Aspect ratio is a characteristic that influences the properties of the nanorods, such as the optical character (Figure 2.3). In nanorods, there are two modes (longitudinal and transversal) of SPR because of the nonsymmetrical shape, which means, there are two resonance wavelengths causing SPR instead of just one for spherical metal nanoparticles (Figure 2.4). These wavelengths can be tuned by changing the aspect ratio of the nanorods, causing a change in the transmitted colour. [26]

There are multiple applications of AuNRs, some of them related to the optical properties through the plasmon resonance frequency. This frequency is quite sensitive to the particle environment, making them a suitable material for biological sensing. [27] As with AuNPs, the AuNRs are also utilizable in phototherapy, because of their ability to transform infrared light into heat. [28]

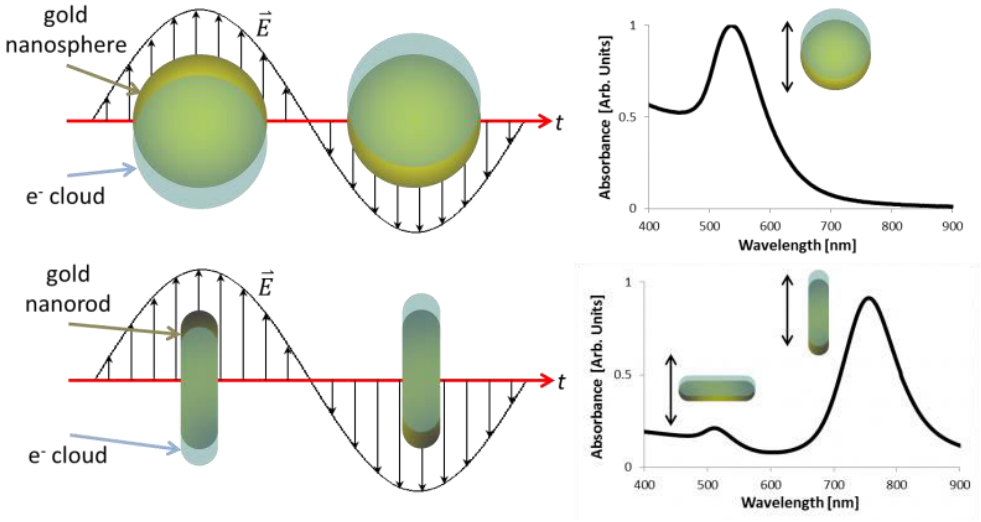

Figure 2.4: *Surface Plasmon Resonance (SPR) effect, where the electrons in the nanoparticle conduction band oscillate in resonance with incident light. The light is absorbed at the resonance frequency. Because of their asymmetrical shape, two resonance frequencies can be found, which correspond to longitudinal SPR (right peak in the absorbance graph for nanorods) and transversal SPR (left peak in the absorbance graph for nanorods). Picture from https://static.scholar.harvard.edu/files/styles/os_files_xlarge/public/ndurr/files/spr_for_gns_and_gnr.png?m=1388882277&itok=VMIlAbd4*

Because of the extensive use of AuNP in biology and medicine, their toxicity and biocompatibility is a target of interest. These properties, as others, depend on the nanoparticle size and are described in the previous chapter. [29]

Silver nanoparticles (AgNPs) share a lot of properties with their golden counterpart. Their use in the biomedical field is widespread, mainly because of their antibacterial and antifungal properties [30] [31]. Apart from biomedicine, where their antibacterial and antifungal properties are utilized, also electronics [32], photonics [33] and other fields draw from the qualities of this material. In recent years, the use of AgNPs in diagnostics and therapeutics is also studied with promising results. [34]

2.3. Particle size characterization techniques

There are multiple techniques that can be used for nanoparticle characterization. They can be either microscopic, such as TEM, SEM or AFM, or based on some physical properties of the

nanoparticles, like optical qualities, mass and others, some of the methods even combining more properties. This chapter focuses on the summary of the common and some less common techniques that can be used for nanoparticle size characterization. [35] [36]

In general, spherical nanoparticles are characterized using their diameter, whereas nanorods using their aspect ratio, which is calculated using the following formula

$$AR = \frac{long}{short}, \quad (1)$$

where long is the long axis of the nanorod and short is the short axis.

2.4. Microscopy techniques

Various microscopy methods can be used; however, wavelength limits the use of optical microscopes when measuring particles in the nano range. Other modalities have therefore been introduced, not based on optics, which can be used for nanoparticles imaging. The ones most used are Transmission Electron Microscopy (TEM), Scanning Electron Microscopy (SEM) and Atomic Force Microscopy (AFM).

2.5. Transmission Electron Microscopy

TEM is a technique using an electron beam, rather than light beam, to interact with the sample. The sample must be thin, so that the beam can pass through and form an image of the specimen. Because of the use of electrons, the basic measurement must be carried on in vacuum, so that the electrons do not interact with the environment before hitting the sample. However, there are newer more complicated techniques allowing measurements in other environments (Environmental TEM). [37]

There are high demands for the sample, it must be thin enough (less than 1 μm), it must withstand the high vacuum during measurements and the electron beam. Sample preparation (and requirements) along with the cost and longer experimental time are the main disadvantages of TEM.

2.6. Scanning Electron Microscopy

SEM is a scanning method using a beam of electrons to scan over the specimen surface and collect data for each point. The electrons interact with the sample in numerous ways and the products of these interactions are detected and sorted giving information about the topography and composition of the sample. The basic structure of a SEM is given in Figure 2.5. Again, as in TEM, the basic SEM is conducted in high vacuum, modern techniques as in TEM allowing environmental measurements. Since nonconductive samples tend to charge under the beam of electrons, one of the sample preparation steps is coating with conducting materials. For conducting specimen, this step is skipped. [37]

The most common SEM signal used, are secondary electrons emitted by the sample. These give an information about the sample topography, where steeper surfaces emit more secondary electrons due to the increase in interaction volume. Edges and steep surfaces are thus brighter in the resulting image. Another signal measurable using SEM is from the back-scattered electrons, which are a product of elastic scattering within the sample. These, along with characteristic X-rays also produced during the measurement, provide information about the elements distribution in the specimen. [38]

TEM can be incorporated into SEM instrument by adding a detector on the opposite site of the specimen. Since TEM has a higher resolution power, while SEM enables measurements of larger samples and 3D measurements, this combination increases the potential use to more possibilities. [39]

The disadvantages of SEM are virtually the same as in TEM, sample preparation, cost and long experimental time.

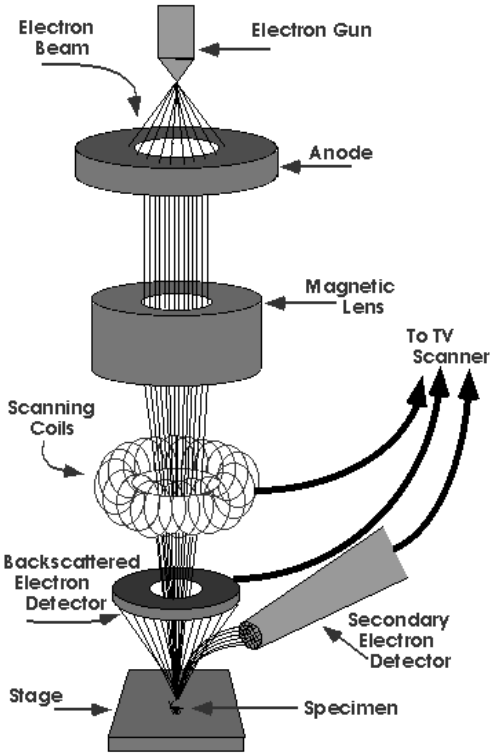

Figure 2.5: *The anatomy of a SEM. An electron beam is shot to a single spot on the specimen and there it interacts. Secondary electrons emitted from the specimen, are detected and give an information about the topography of the sample. Backscattered electrons give an information about element distributions in the sample. Other detectors can be included. The whole process is held in high vacuum. Picture from https://www.purdue.edu/ehps/rem/rs/graphics/sem2.gif.*

2.7. Atomic Force Microscopy

Since one of the main techniques used in this work is AFM, it will therefore be discussed in a deeper manner. AFM is a scanning microscope with down to atomic resolution based on physical interaction of a cantilever tip and a sample. Due to forces between the tip and the sample, the cantilever bends (Figure 2.6A) and this bending is visualized using a laser beam (Figure 2.6B). From the laser position on the photodetector, the force can be calculated and thus the distance between the tip and the sample can be measured. AFM nowadays works in constant force regime, where a feedback controls the cantilever bending and changes its *z*-position to maintain constant force (in other words to undo the cantilever bending). A map of the *z*-positions of the cantilever then corresponds to the topography of the sample. [40] [41]

The force F (N) applied to the surface of the sample by the probe can be calculated using Hook's law:

$$F = -k \cdot D, \tag{2}$$

where k (n/m) is the probe force constant and D (m) is the deflection distance. [40]

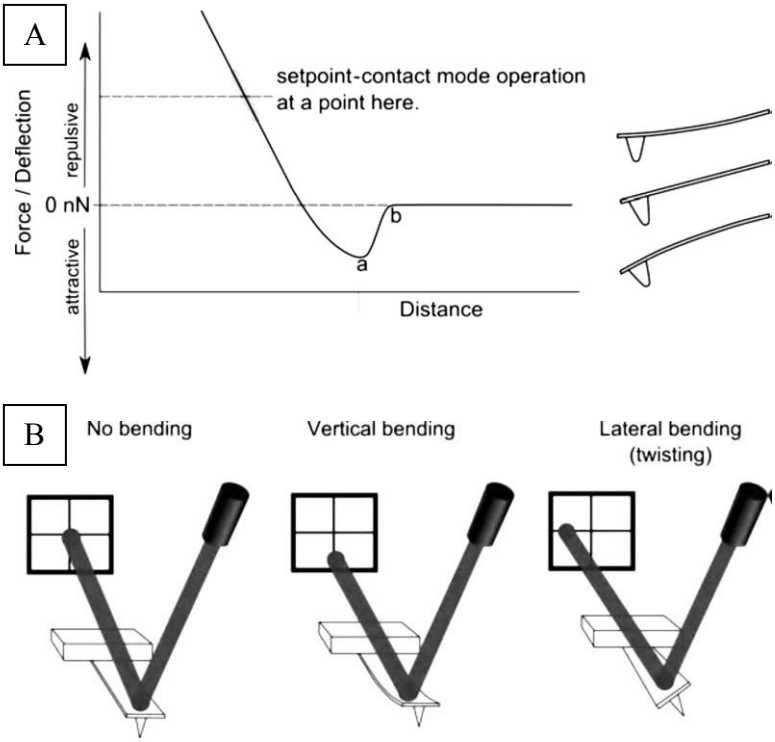

***Figure 2.6**: A) A simplified force-distance curve of an AFM. As the cantilever is coming closer to the surface, attractive forces (van der Waals forces) are pulling the tip to the surface, thus bending the cantilever. As the cantilever comes closer, repulsive forces push the tip away, which again bends the cantilever. B) how the cantilever bending affects the laser beam position on the photodetector. Pictures from [40].*

There are two main AFM topographic measurement modes – contact mode (also tapping, intermittent contact) and oscillating mode (also non-contact or close contact). In contact mode, the tip is in contact with the sample the whole time (meaning there is a constant force applied by the tip to the sample) and the topography is calculated from the z-position of the cantilever. In non-contact mode, the cantilever oscillates at resonance frequency above the sample. The forces between the sample and the tip change the amplitude and phase of the oscillations in dependence on the tip-sample distance (Figure 2.7). Here again the feedback maintains constant force, reacting to the changes in amplitude and phase. [40] [41]

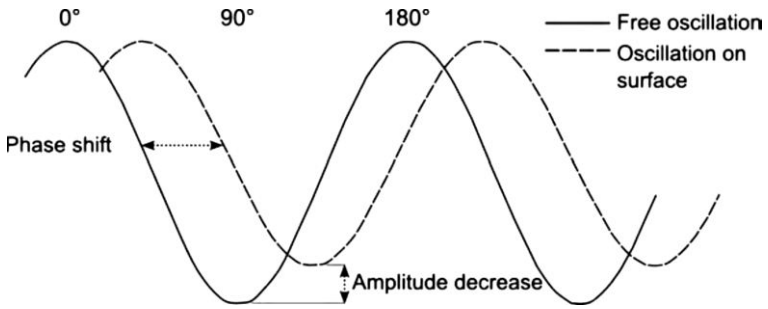

Figure 2.7: *Cantilever oscillation away from surface (full line) and in contact with the surface (dashed line). Picture from [40].*

There are other non-topographic modes in AFM, which give information about the mechanical, electric, magnetic and other sample characteristic. These depend among others on the probes used. It is also possible to used AFM as a surface or particle manipulation tool. [42] [43]

To measure the topography of a sample using AFM, certain preparation is needed. The sample must adhere to the substrate, so that it doesn't move during the measurement. The more rigid the sample, the easier the measurement (for less rigid samples the scanning probes must be very soft, so that they bend more, which means that the applied force is smaller – formula 1). There are also dimensional restrictions for the sample. Most AFM have a maximal scan range in the sample plane (x-y plane) 100x100 μm and a maximal z range of 10 – 15 μm. [44]

For the best possible quality image optimizing scan conditions is crucial step while imaging using AFM. Apart from physical optimization, like choosing a right probe for the application, ensuring the probe is sharp and others, there are also multiple software adjustments. All these are made while scanning and observing the system work. The first step is to find the optimal feedback, where the system reacts appropriately to a change in the sample topography. A gain too high will cause oscillations of the probe, whereas a gain too low results in the probe not following the sample topography, as shown in Figure 2.8. Another parameter to adjust is the set-point, which controls the force between the probe and the specimen. The lower the set-point, the smaller the force, which is usually preferred, however sometimes a greater force is needed. The last discussed parameter is the scan speed. The slower the scanning, the better the imaging, because the system has more time to react to changes in the sample topography. The time of the experiment is then increased, an optimal speed is therefore sought. These three parameters

correlate with each other. For the same image quality one can slow down the scan speed and increase the gain as well as the other way round. Until the gain is too high. [40] [45]

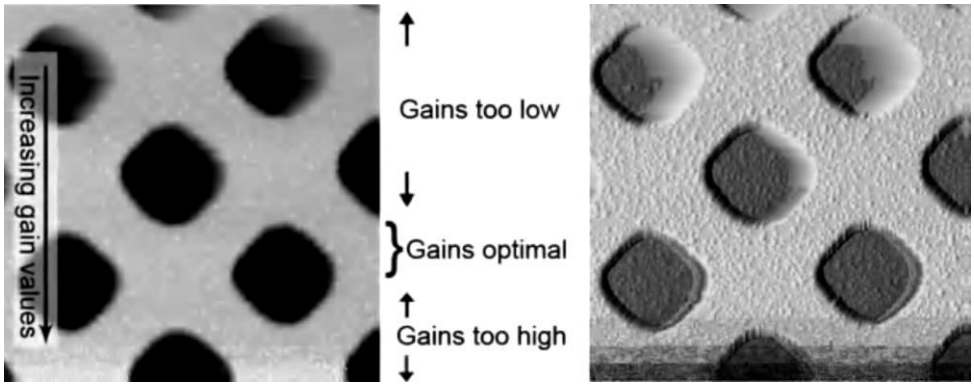

Figure 2.8: *The effects of different feedback setting on the image. A low gain results in a blurred image (upper part of the images), gain too high causes oscillations of the cantilever (lower part of the images). Left is height image, right is error image. Picture from [40].*

One of the challenges, when measuring with AFM, is the fact that the resulting picture is not a true image of the sample, it is rather a convolution of the tip and the sample topography (Figure 2.9). Most cantilevers report a tip dimension less than 10 nm, this however changes during the measurement, because the tip wear out. For samples big enough (in the micrometre range, such as cells), the tip contribution is almost neglectable. For nanoparticles, however, the tip convolution results in a visibly enlarged image in the x-y plane. Therefore, a deconvolution must be employed, if the exact size is to be determined. For the determination of the diameter of spherical nanoparticles, the deconvolution is not necessary, since the particle is symmetrical and its height, which is measured as z-position of the tip, corresponds to the diameter itself (red line in Figure 2.9 as topography depicts the exact height of the sphere, but the horizontal size is enlarged). [40] [46]

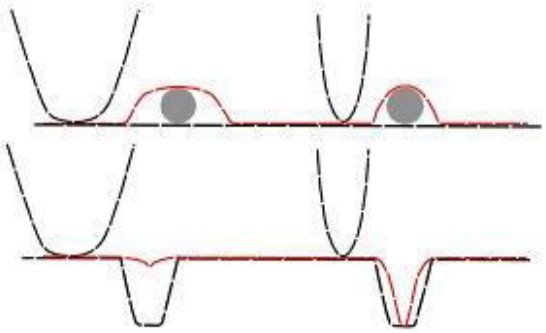

***Figure 2.9**: Cantilever convolution with the sample. A sample, such as a sphere (grey circle) or a dent is measured using a tip. The wider the tip, the more distorted is the image. The resulting profile is depicted in red. Picture from http://afmhelp.com/images/stories/conv_small.jpg.*

AFM UTILIZATION IN A NANOSENSORS FOR BIOMEDICINE LABORATORY

Apart from size and shape determination, the AFM has been used in our laboratory (Nanosensors for biomedicine at FBMI CTU) for multiple purposes. Some of them being determination of surface roughness of nanolayers (Figure 2.10), imaging of fixed cells (Figure 2.11) or determination of the effect of glass functionalization on the deposition of nanodiamonds.

More potential uses of the AFM are based on other measurement modes, such as force spectroscopy (FS), where the tip is pushed into the sample and away again and the forces on dependence on the tip-sample distance are measured. FS can be used either for the measurements of membrane mechanical properties and their change during interactions with nanoparticles or for the detection of forces between different biological elements, where one of them is attached to the cantilever and is brought nearer and taken away from the other.

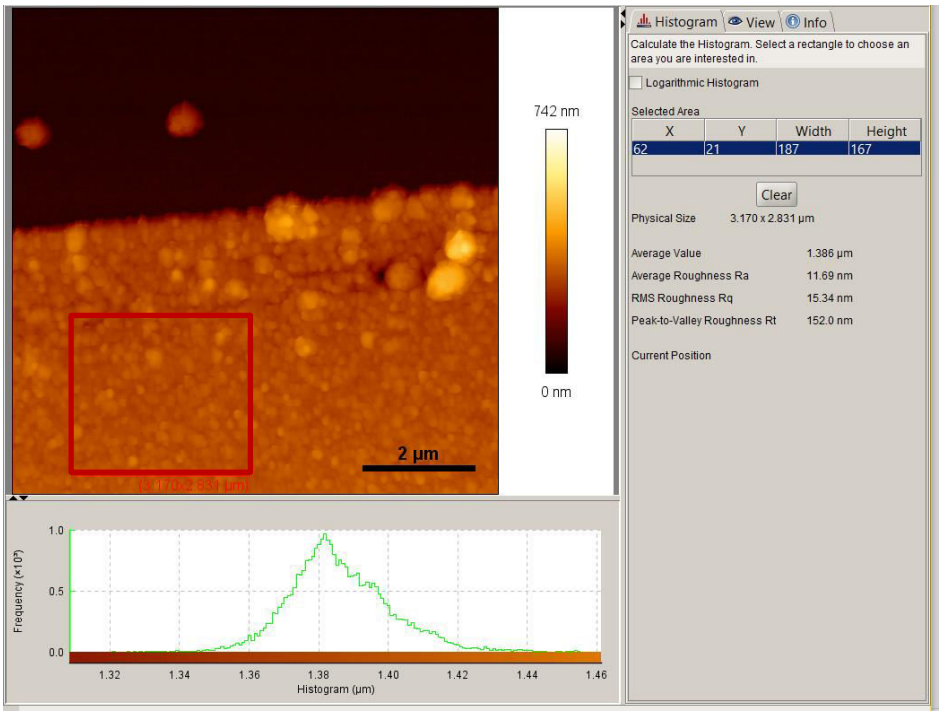

***Figure 2.10**: AFM image of a nanodiamond layer. The roughness can be calculated from a chosen area (red square) and displayed in the JPKSPM Data Processing program. Here, the average roughness is 11.69 nm. Image taken in the laboratory Nanosensors for biomedicine.*

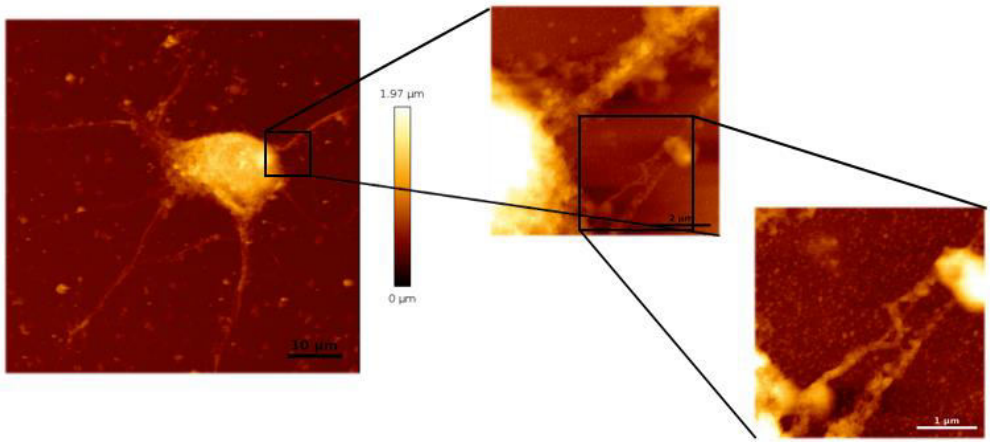

***Figure 2.11:** AFM height image of a fixed neuron cell. The close ups represent the possibility of imaging only regions of interest, once they are found in the sample. Images taken in the laboratory Nanosensors for biomedicine.*

AFM is in comparison to the other microscopy techniques considered cheaper, faster and easier to work with because of the easier sample preparation. Another advantage of AFM in

comparison to the other microscopic techniques mentioned above, is that it is also utilizable when measuring biological samples in different environment, air or liquid and that it can be used for other than topographical measurements as well. [40]

2.8. Dynamic Light Scattering

Dynamic light scattering (DLS) being the second main method of particle size determination in this work, will be discussed deeper as well. It is a method used to determine size distribution of nanoparticles in suspensions. It is based on the fact that particles, which are small enough (less than 10 μm), in suspensions undergo Brownian motion. The larger the particle, the slower it moves. A laser beam is shot through the sample where it interacts with the particles suspended in the solution and produces a scattering pattern (Figure 2.12). [47] [48]

The fluctuation of light intensity for a given scattering angle is monitored in time, giving a signal, which correlates with the particle size. Bigger particles move slower; the fluctuations are therefore slower in time. Smaller particles produce more rapid changes in the intensity fluctuations in time (Figure 2.13). [47]

From the intensity fluctuations in time a second order autocorrelation function $g_2(\tau)$ is derived as stated:

$$g_2(\tau) = \frac{G_2(\tau)}{\langle I \rangle^2}, \quad (3)$$

where $G_2(\tau)$ is the temporal correlation function (it correlates the intensities in time t and $t + \tau$), $\langle I \rangle$ is the average intensity and τ is the correlation time. [49]

From the second order autocorrelation function, the first order autocorrelation function $g_1(\tau)$ can be derived, which then gives the diffusion coefficient:

$$g_1(\tau) = e^{-q^2 D \tau}, \quad (4)$$

where q is the magnitude of the scattering vector (see Figure 2.12) and D is the diffusion coefficient. [49]

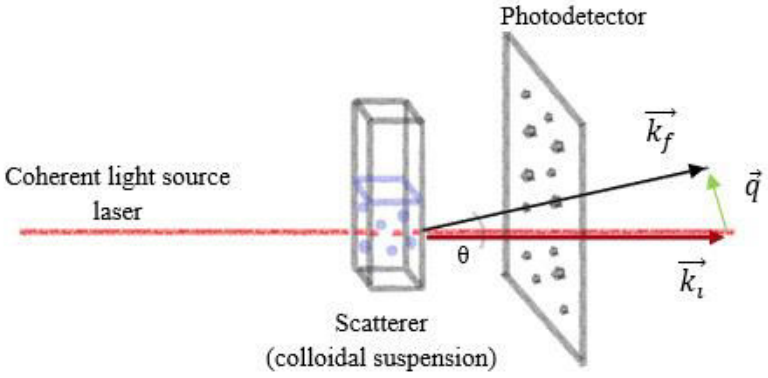

Figure 2.12: *Principle of DLS. The light from a coherent light source passes through a sample and is scattered. The scattered pattern is detected with a photodetector and further processed.* θ *is the scattering angle,* $\overrightarrow{k_i}$ *is the incident wave vector,* $\overrightarrow{k_f}$ *is the scattered wave vector and* $\vec{q}$ *is the scattering vector given by the difference between the wave vectors. Picture inspired by https://www.deutsche-digitale-bibliothek.de/binary/3XOAXSCVG7RB4ZEN3O44E7M6PUSFNPTX/full/1.pdf*

The nanoparticle size is then obtained using the Stokes-Einstein law:

$$D = \frac{kT}{6\pi\eta R_H} \tag{5}$$

where k is Boltzman's constant, T is the thermodynamic temperature, η is the viscosity of the solvent and R_H is the hydrodynamic radius of the particles. [49]

The DLS instrument shows the results as a size distribution by intensity. From this distribution, the Z-average size is calculated by the instrument. Z-average is the mean size as weighed by intensity. This is the preferred DLS size parameter, since it is insensitive to noise. Another value that is of importance is the polydispersity index PdI, which is defined as:

$$PdI = \left(\frac{\sigma}{d}\right)^2 \tag{6}$$

where σ is standard deviation and d is the Z-average size. [50]

PdI describes the uniformity of the sample. The higher the index, the less uniform the sample is. In general, samples with PdI bellow 0.1 are considered monodisperse and vice versa, samples with PdI above 0.1 are referred to as polydisperse. [50]

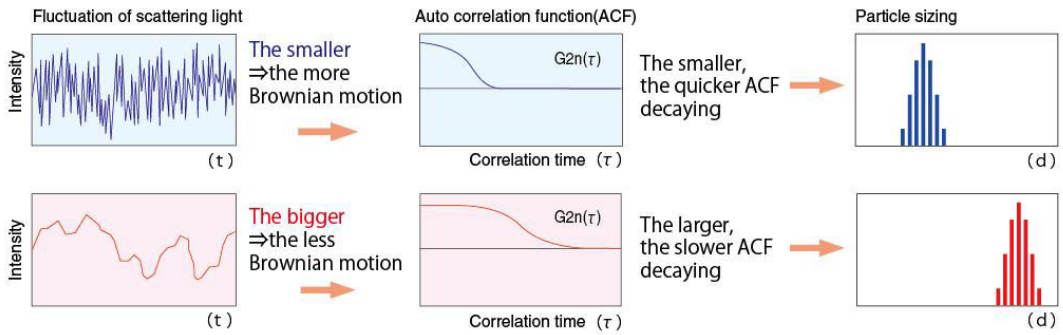

Figure 2.13: *The intensity fluctuations in time for a given scattering angle for big and small particles and the autocorrelation functions calculated. Depending on the speed, with which the Autocorrelation function decreases, is the particle size. Picture from https://www.otsukael.jp/upload/files/ELSZ-2000-2E%281%29.jpg*

The particle size, which is derived from the DLS measurement is in fact not the true size, but rather the size of a sphere, which will give the same scattering pattern as the particles. Another limitation is that the method considers a so called solvation layer around the particle to be a part of it. A solvation layer is a shell around a suspended particle, consisting of the molecules of the solvent. Because of this, the particles, when measured using DLS, look bigger, than their actual size.

When measuring non-spherical samples (like rods, as in this work) the equations become more complex, since the rotational movement must be taken into consideration. In the case of nanoparticle rods there are in fact two diffusion coefficients – rotational D_r and translational D_t. Also, their anisotropy is not negligible, leading to two autocorrelation functions for a VH and VV geometry (vertical polarization of incident light and horizontal/vertical detection). There are more (two) relaxation modes in the intensity correlation function (Figure 2.14). Several methods can be used to process the data. One of them being nonlinear least-squares fit of the autocorrelation functions to determine the two diffusion coefficients and from there the geometrical particle parameters - their length L and aspect ratio L/d can be estimated. [51]

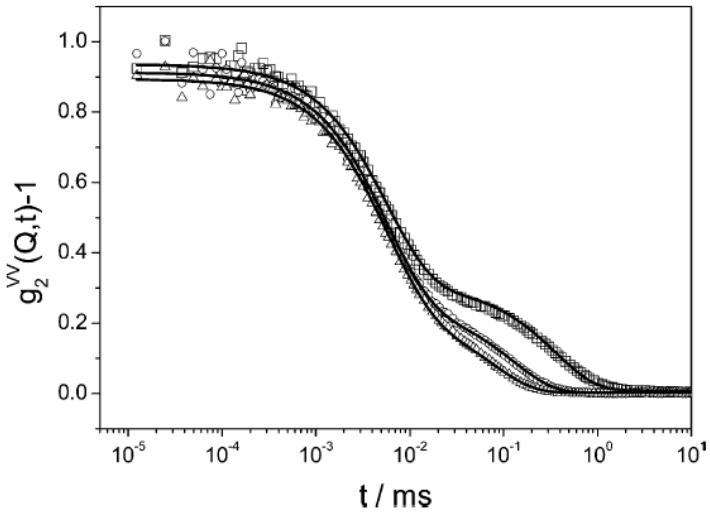

Figure 2.14: *The two relaxation modes (two "hops" in the curve) in the autocorrelation function of golden nanorods for the VV detection geometry. The three functions are for three scattering angles 40°, 90° and 130 °. Picture from [51].*

For the mentioned exact determination of nanorod aspect ratio more complex DLS equipment has to be used, where the scattering is measured under multiple angles. In most cases, however, the user has a basic instrument, where only one scattering angle is measured. There, the precise size characterization for nanorods is not available. The two diffusional coefficients – rotational and translational – yield a bimodal size distribution by intensity. It can be said that the bigger the nanorod aspect ratio, the bigger is the contribution of the rotational movement (Figure 2.15). [52] The relative size of the two peaks could thus be used for an approximate determination of the nanoparticle aspect ratio. However, for an unknown sample, the bimodal distribution could also mean a polydisperse sample consisting of two spherical nanoparticles. [53]

DLS is not very suitable for measurements of polydisperse samples. The bigger particles overlay the smaller, so for the small nanoparticles to have a sufficient detectable scattering intensity, their fraction in the sample must be very high in comparison to the larger ones. Also, the data interpretation is quite demanding. [53]

On the other hand, DLS is a quite fast method for measurement, it is cheap and the sample preparation is relatively easy.

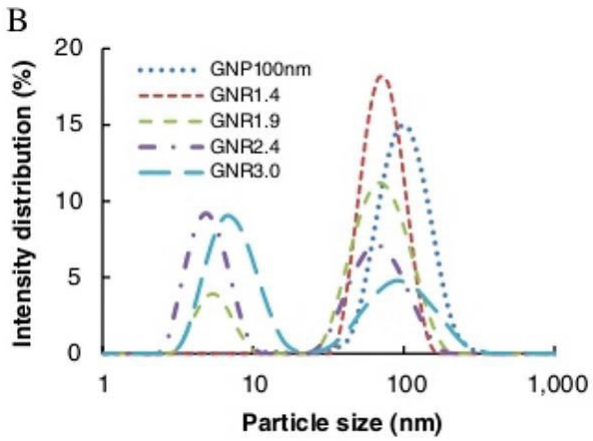

Figure 2.15: *DLS size distribution for nanoparticles of spherical (blue-dotted line) and rod-like shape. The larger the aspect ratio, the bigger is the contribution of the rotational movement (the intensity of the first peak). Picture from [52].*

2.9. X-RAY DIFFRACTION

Another method for nanoparticle size determination in powder modification is X-Ray Diffraction (XRD), where a beam of X-rays is sent to a powder sample and is scattered by the atoms. The resulting scattering pattern is produced by interference of the scattered X-rays. To obtain the particle size out of the scattering pattern, different calculation methods can be utilized, such as the Scherrer equation, which correlates the particle size to the width of a peak in the scattering pattern. The main disadvantage of XRD is the fact that the experimental time can be quite long and it needs a large portion of the sample. [54]

2.10. ULTRACENTRIFUGATION

Analytical ultracentrifugation (ANUC) is also a method utilizable for not only nanoparticle size determination, but also the molar mass or particle density. The method is based on observation of the sedimentation process via an optical system. The optical system is used to record the concentration profile as it changes with the distance from the rotor and with time. Numerical models are later used for the determination of the sedimentation coefficient and diffusion coefficient, from which the size of the particles can be calculated. [55]

2.11. DIFFERENTIAL MOBILITY ANALYSER

Differential mobility analyser (DMA) is a method sorting nanoparticles using the fact that nanoparticles of corresponding sizes will have the same electrical mobility. For nanoparticles in aerosol samples, DMA is considered as a primary tool for size characterization. In this method, a charged aerosol is sent into a chamber with applied varying electric field. The particles in the aerosol then move towards the end of the chamber and those of identical sizes arrive at the same time. From this, the electrical mobility distribution can be determined and afterwards also the size distribution. [56]

2.12. IMAGE PROCESSING AND ANALYSIS

From the microscopic measurements, a 2D (or 3D in the case of AFM) is obtained. To get the nanoparticles properties, such as its size, image analysis is needed. The following chapter summarizes the steps needed in the image analysis process used in this work and other possibilities that can be employed in image processing and analysis.

2.13. NOISE REDUCTION

When a raw image is taken, unwanted signals are present. These are often random and can affect the later image analysis. One of the possibilities for noise reduction is using smoothing. In other words, the values of each pixel are averaged according to the values of the neighbouring pixels. This way, small noise signals comprising few pixels vanish. This is done by convolution of the image and a mask, which sets the pixels, from which the average (or weighed average) is calculated. This method is simple and effective, one of its drawbacks being that it results in blurring of the image. [57] [58]

Instead of the average value, median value of neighbouring pixels can be used for noise reduction as well. It performs better for small levels of noise, where it does not result in that much blurring. However, the computational time for this filter is quite long. [59]

An efficient method for noise reduction while preserving the image features is transformation of the image into another domain, such as wavelet. There, the image is decomposed into wavelets where noise is contained in few small coefficients, while the important signal is grouped into few larger coefficients. Thus, it is easier to distinguish the noise and filter it. [60]

When the image is black and white an easy method for removing noise consisting of only few pixels is utilizing morphological operations such as opening and closing. Image opening is a operation, where the image is firstly eroded (the pixel number of each object is decreased) and then dilated (the pixel number of each object in the eroded image is increased) using a structural element, which sets the pixels, which will be taken into account when setting the value of the investigated pixel. Image opening removes noise in the background – it disappears because of the erosion (Figure 2.16). Image closing on the other hand, fills places in the image, where there are discontinuities in the objects (Figure 2.16). Both opening and closing have been used in the image processing program prepared for this work. [61] [62]

Figure 2.16: *Image opening and closing. Left is the original image, in the middle, opening was performed, which led to loss of small features in the image (visible on the feet of the lion). Right is image closing. It leads to filling of the blank spaces in the image. Picture from http://cmp.felk.cvut.cz/~hlavac/TeachPresCz/11DigZprObr/71-3MatMorpholBinCz.pdf*

2.14. IMAGE SEGMENTATION

As the goal of this work was to determine the sizes of nanoparticles, these have to be found in the images taken. Image segmentation is therefore a crucial step. Multiple methods of image segmentation exist.

One of them being segmentation based on edge detection. With the help of edge detection, the boundaries can be found that close around the objects. However, edges appear not only around the objects but also because of other effects, such as illumination (shadows). It is hard to obtain closed boundaries of the objects. [62]

Other methods involve searching for regions with the same property, such as brightness. These are called clustering and assign a pixel to a group of other pixels, if it fulfils a given criterion. The most popular clustering method is the K-means, which is based on the random assignment of k initial means to the image and each pixel is assigned to one of the means, based on its distance from the means. The centroid of the resulting clusters is assigned as the new mean and this process is repeated until it converges. [63]

However, the simplest case of image segmentation is thresholding. This way, the background is distinguished from the objects of interest in the image, if the objects have a sufficient intensity. The image is transformed into black and white image with a threshold set to a certain value. This was also satisfactory for the data analysis used in this work. [62]

2.15. OBJECT SIZE DETERMINATION

Once the image has been cleared from noise and segmented into individual objects, the properties of the objects can be found. The diameter of spherical objects, or the axes lengths of elongated objects can be found by interpolating the objects with ellipses of the same normalized second central moments as the region (Figure 2.18). From there, the ellipse's long and short axes can be assumed to correspond to some extend to the axes of the object. For spherical nanoparticles, both axes should appear the same in size, the aspect ratio distribution would therefore be monomodal with a peak around 1. However, a more precise method for the diameter determination of spherical nanoparticles measured using AFM is to detect the height of each object.

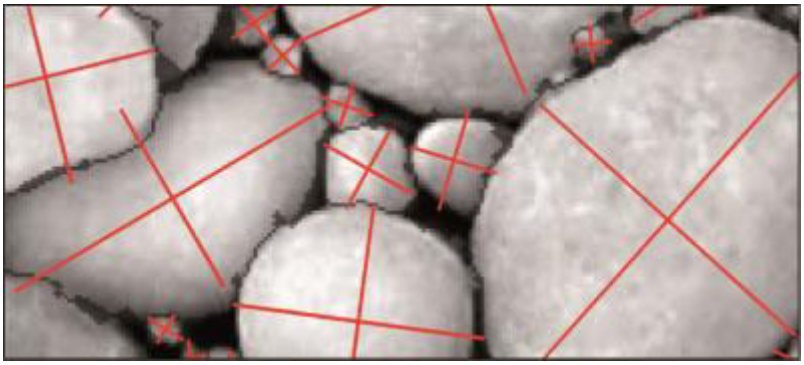

Figure 2.17: *Image with depicted object axes calculated by MATLAB from the interpolation with ellipses of the same normalized second central moments as the regions of interest. Picture from https://www.researchgate.net/profile/Martin_Detert/publication/283879329/figure/fig3/AS:391565685084162@1470367942252/Figure-5-Final-result-of-object-detection-procedure-Straight-lines-colorprint-red.jpg.*

2.16. STATE OF THE ART

The following chapter describes the state of the art in nanoparticle size and shape determination using different techniques.

Multiple methods have been compared in relation to nanoparticle size determination. The methods used in this work (AFM and DLS) included. All of the mentioned studies have been executed on spherical nanoparticles of different materials.

DLS, AFM and X-ray diffraction have been compared by measuring magnetite nanoparticles of around 11 nm. The results of this study suggest that all three methods are comparable when determining size distribution. However, DLS exhibits lesser sensitivity for smaller nanoparticles in the case of wider size distribution. XRD is presented as a classical method with a complex data analysis. Despite the drawbacks of AFM being the tip finite dimension and its effect on the resulting image, this method is complementary to the other methods with an additional use for nanoparticle shape analysis. [64]

Another study compares AFM and DLS for size determination of nanoparticles of 20 nm, 100 nm and their mixtures (8:1, 5:1 as 20nm:100nm). Both techniques were comparable as to the size determination of monodisperse samples. DLS was reported to not be suitable for measuring mixtures. In both mixtures, the size distributions were distorted and not corresponding to the sample. AFM on the other hand provided bimodal size distributions with quite accurate results. [49]

DLS was further compared to electron microscopy and ultracentrifugation on spherical poly(butyl cyanoacrylate) nanoparticles. The results showed that electron microscopy (specifically SEM) is the technique, which gives the most direct information about the size distribution and shape of the nanoparticles. The main disadvantage of SEM is the possible change in particle properties during the sample preparation, mostly their shrinkage. DLS is represented as a fast and relatively low cost technique. The results from a DLS however show a shift in the size distribution towards bigger values, which is due to non-direct determination of the size. The resulting diameter is that of a sphere which yields the same diffusion coefficient as the nanoparticles in the sample (see 2.8). Ultracentrifugation has been shown to provide comparable results with both DLS and SEM. [65]

3. AIM OF STUDY

The aim of this study is to use two methods for size distribution analysis – AFM and DLS – and to compare and discuss their suitability for particle size and shape characterization. Both methods were used on AuNP and AgNP samples of spherical and rod-like shapes.

The specific objectives of this study were:

- Optimization of AFM measurements on a reference sample
    - In air
    - In water
    - Contact mode
    - Non-contact mode

- Size and shape characterization of AuNP and AgNP mono- and polydisperse samples
    - Using AFM
        - Data analysis using own MATLAB program
    - Using DLS
        - Data analysis using Zetasizer software
    - Using TEM/SEM as control
        - Data analysis using ImageJ program

- Comparison and discussion of the two used methods and TEM/SEM as control

4. Equipment and Methods

In the following chapter the equipment and methods of preparation of the samples for the individual measurements are summarized as well as the materials. The nanoparticle samples (Figure) were a kind gift of the Institute for Experimental Physics from Free University Berlin.

4.1. Transmission Electron Microscope

In our study TEM/SEM was used as a reference method for the determination of sample size distribution and shape. Samples were measured in Berlin at the Free University Berlin at the Institute for Experimental Physics. High resolution TEM was performed employing an imaging-side aberration-corrected FEI TitanCube microscope working at 80 kV, equipped with a Cs corrector (CETCOR from CEOS-60/65-GmbH).

Figure 4.1: *Nanoparticle samples. Left to right: AgNP, AuNP, AuNR long, AuNR short.*

4.2. SAMPLE PREPARATION – REFERENCE AFM MEASUREMENTS

The reference sample – Au-projection-pattern of 356 µm – was obtained from kentax.de and measured in air and water using contact and non-contact modes. All AFM images were measured on an JPK NanoWizard 3 ® AFM in either contact or non-contact mode. Cantilever holder for non-contact measurements with external drive was used in all measurements.

MATERIALS:

Au-projection pattern (356 µm) – Kentax GmbH

***Table 4.1**: Cantilevers used for the different measurement modes*

Contact mode	Air	HYDRA2R-100N AppNano
	Water	HYDRA6V-200W AppNano
Tapping mode	Air	Tap300Al-G Budget Sensors
	Water	HYDRA6V-200W AppNano

PROTOCOL:

The reference sample was glued to a cover glass (25 mm) and mounted in a holder to minimize disturbances. In air the sample was measured using the listed cantilevers. For the water measurements, the sample was immersed in dH_2O. When measuring in tapping mode, the approach was firstly done in contact mode, then the tip was retracted and the resonance frequency set in the JPKSPM software.

4.3. NANOPARTICLE SAMPLE PREPARATION – AFM

MATERIALS:

Distilled water, demineralized water

AuNP sample – 15 nm

AgNP sample – 50 nm

AuNR sample – long

AuNR sample – short

Cover glasses – 25 mm

NaOH

PROTOCOL:

Since the nanoparticles are in a hydrophilic form, a highly hydrophilic glass cover was prepared by cleaning 25mm glasses.

For the glass cleaning, 5 g of NaOH was diluted in a small amount of dH_2O in a beaker, the glasses were immersed in a holder and the beaker was filled above the holder with 96% ethanol. The solution was slightly heated and stirred for two hours and left overnight. Then the glasses were thoroughly cleaned with dH_2O and if not used immersed in $demiH_2O$.

The samples were firstly diluted in dH_2O to create a 6% solution – 10 µl of NP solution with 590 µl dH_2O. Following sonication for 10 minutes, 200 µl of the diluted solution was drop casted on clean glass and left to dry.

The samples were then measured in non-contact mode using cantilevers Tap300-Al-G by Budget Sensors. Images were measured with gain around 400, relative set point was held below 80 %.

4.4. SAMPLE PREPARATION – DLS

EQUIPMENT:

The sonicators used were Bandelin Sonorex RK31 for AuNP and Elma Elmasonic P D7824 Singer. Samples were centrifuged using Eppendorf 5430R at 20 °C. For our study the Nano ZS zetasizer system by Malvern Instruments was used.

MATERIALS:

AuNP sample – 15 nm

AgNP sample – 50 nm

AuNR sample – long

AuNR sample – short

Distilled water

PROTOCOL:

The samples for DLS were firstly sonicated for 10 minutes (AgNP, AuNRs) or 20 min (AuNP). To get rid of larger impurities, the samples were centrifugated for 3 min with rcf of 30g. The samples were then again sonicated for approximately 1 minute, diluted to 10 % (0.5 µl of particles in 49.5 µl of dH_2O) and loaded into quartz microcuvette.

Samples were measured using Nano ZS zetasizer system by Malvern Instruments. The fixed scattering angle was 173°, measurement temperature was 25°C, laser wavelength 633 nm. Samples were measured in water. The integration time was set to 10 s.

For the small AuNP, longer integration time (100 s) was used with the same preparation.

Each sample was measured in three cycles, the minimal intensity of the signal required for the measurement was considered 150.

4.5. MATLAB PROGRAM

For the data analysis of the AFM images, a program in the software MATLAB was programmed. The functions are summarized in the following chapter – Results. Image data were first modified using JPKSPM Data Processing program, where the only operations conducted were subtraction of polynomial fit from each scan line independently and then subtraction of a polynomial fit from each scan line using a limited data range (Degree 1, Lower Limit 0 % and Upper Limit 70 %). The resulting image was exported to ASCII format and this was used as an input for the prepared image analysis program. The resulting diameters and aspect ratios were transferred into excel and the statistical analysis was performed there. Figure 4.1 demonstrates the undertaken steps during the data processing.

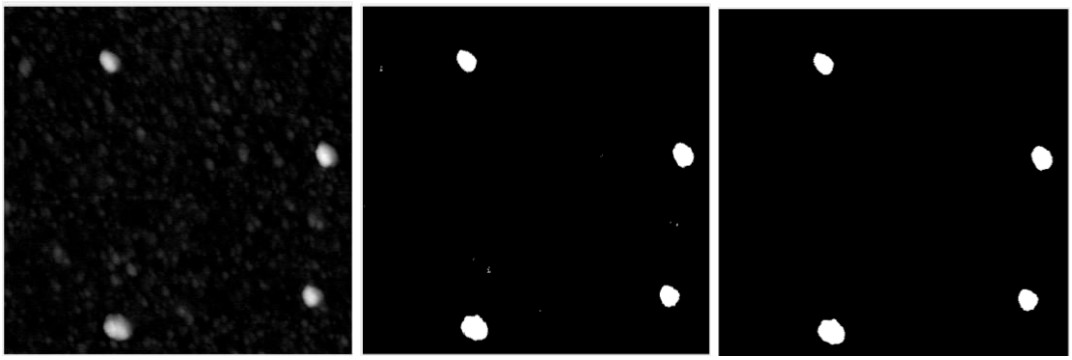

Figure 4.2: *Steps required in the data analysis. On the left, the uploaded image in grayscale, with four visible nanoparticles. The image was segmented using a threshold. Noise is still visible as white dots in the background. On the right is the same image with removed noise by opening (eliminating the white dots) and closing of the image.*

4.6. STATISTICAL ANALYSIS

The results from DLS were extracted and plotted in the Malvern Zetasizer program. The nanoparticles from TEM images were manually measured in the ImageJ program (Figure 4.2 demonstrates the manual measurements of nanorods) and calculated using excel. For the nanorods, only rods were measured, not spherical particles, which were also present in the samples. Results from DLS are expressed in Z-average and polydispersity index PdI, which is defined by formula 6. The diameter results from AFM and TEM/SEM are expressed as mean ± standard deviation. There, mean was determined using the formula:

$$\bar{x} = \frac{1}{N}\sum_{i=1}^{N} x_i, \tag{7}$$

where $\bar{x}$ is the mean diameter, x_i are the measured diameters and N is the number of measured diameters.

The standard deviation σ was calculated using the formula:

$$\sigma = \sqrt{\frac{\sum_{i=1}^{N}(x_i - \bar{x})^2}{N-1}}. \tag{8}$$

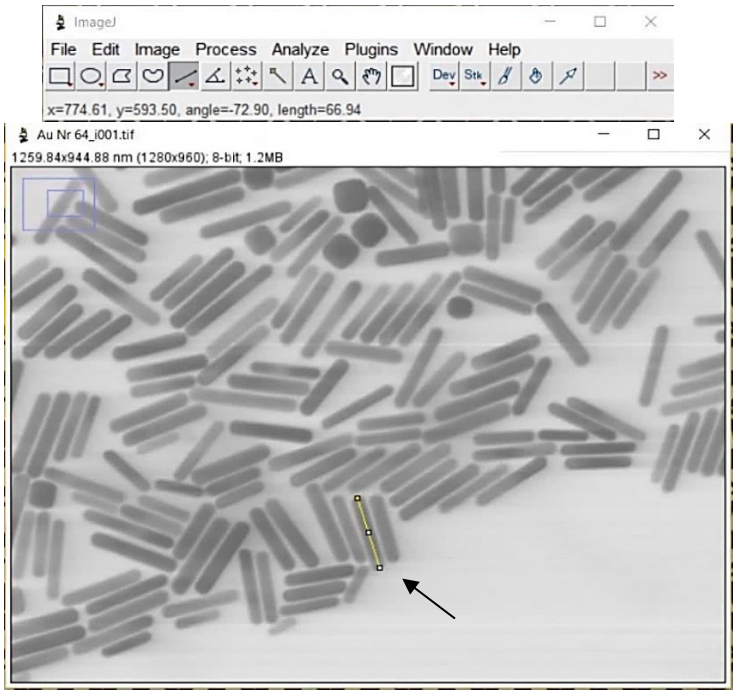

***Figure 4.3**: Manual measurements of nanorods dimensions from TEM/SEM images using ImageJ software. The yellow line (pointed) demonstrates the measured long axis.*

5. RESULTS

In the following chapter, the results are summarized, including the reference sample measurements for AFM imaging optimization, nanoparticles measurements using AFM and DLS and the AFM image analysis.

5.1. AFM MEASUREMENT OPTIMIZATION

AFM offers down to atomic resolution, when the right settings of the program and suitable equipment is used. Different modes of topography measurements (tapping and contact) are possible to employ, each one of them presenting new possibilities but also requirements. AFM also enables measurements in different environments, for example air and water. For the further experiments, each kind of measurement was optimized to obtain an image with a resolution as high as possible with the cantilevers available.

Results are shown in the Figures 5.1 – 5.3 bellow. The result show that each one of the measurements yields comparable resolution.

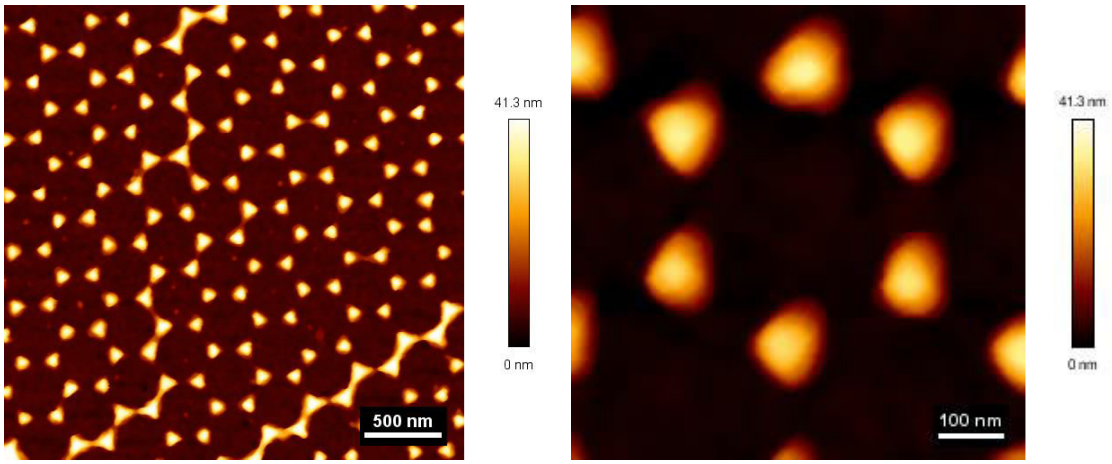

Figure 5.1: *AFM height images of reference sample measured in contact mode in air using HYDRA2R-100N cantilever. Right is a close up of the reference sample.*

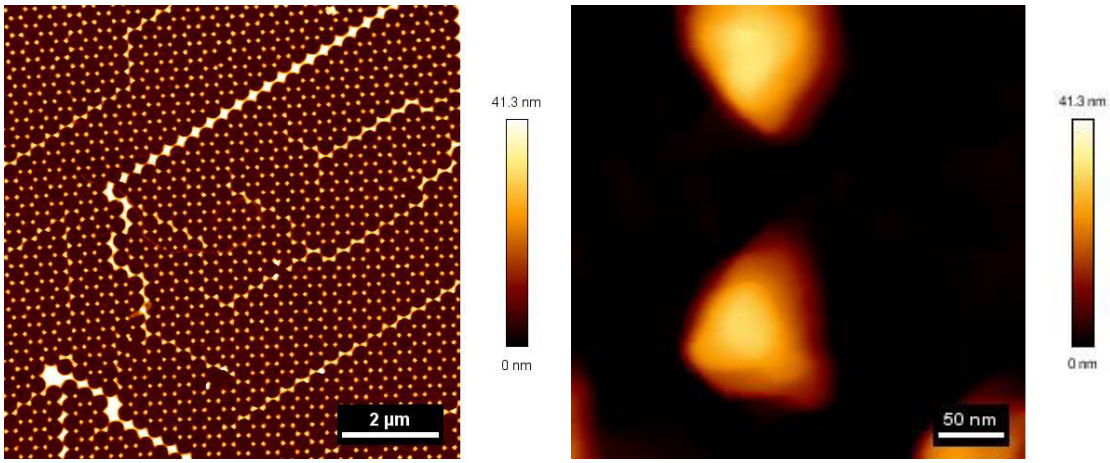

Figure 5.2 : *AFM height images of the reference sample measured in non-contact mode in air using Tap300Al-G cantilever. Right is a close up of the sample.*

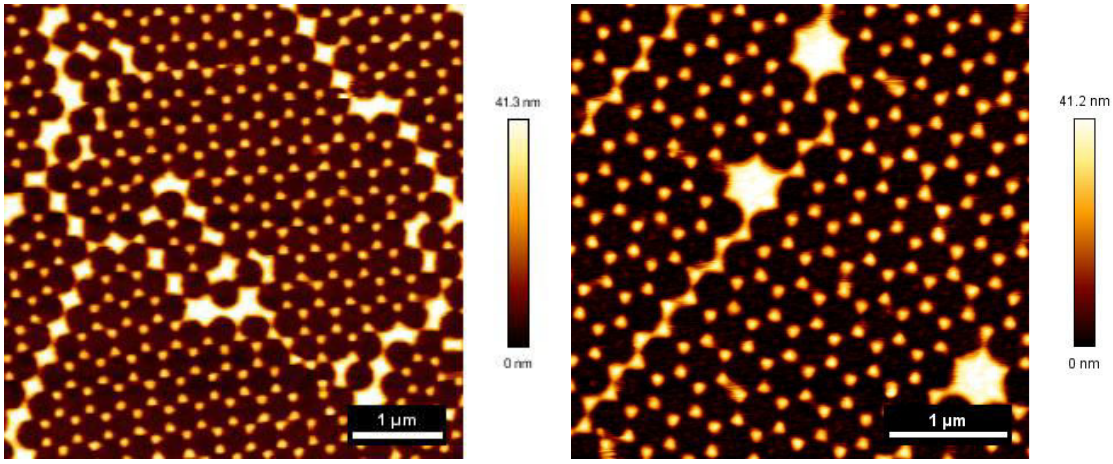

Figure 5.3: *AFM height images of the reference sample measured in water. Left image is from contact mode measurement, right is from non-contact measurement, both performed using HYDRA6V-200W cantilever.*

For further measurements tapping mode was chosen because of its small interaction with the sample and much easier and faster measurement. The measurements were decided to be held in air, since water brings more aspects to the process and the measurements are more sensitive to noise.

5.2. MATLAB ANALYSIS PROGRAM

For the nanoparticle size determination, a program in MATLAB software environment was programmed.

The algorithms for the program are shown in Figure 5.5. The loading part was written by Ing. Martin Otáhal, who gave a kind consent to use it.

Images were loaded in ASCII format. The previous processing in the JPKSPM Processing program was limited only to the operations mentioned above (see 4.5). If any other operations were involved, the head of the ASCII file changes and the variables are not loaded correctly.

Due to possible aggregates in the images, a crop function was added in both programmes to choose only individual particles (if distinguishable).

For spherical nanoparticles, the images were first transformed into black and white images with an automatic threshold determined by MATLAB. Thresholding was also used as image segmentation operation. To get rid of remaining artefacts and noise, image opening and closing was applied. Each segment was labelled and the highest z-value in each segmented particle was found, which corresponds to the height of the nanoparticle. Since the particles are spherical, the z-size also corresponds to the diameter of the particle. Because of the limited amount of particles in one image, the program works in a loop, where the user has to determine, whether another image will be loaded or not. The output is a diameter expressed as mean ± standard deviation. The diameter results for all measured nanoparticles are saved in a table, which was afterwards copied to excel for graph formation.

The first part of thresholding, noise removal and object labelling was the same for nanorods. The z-size in this case is supposed to correspond to the short axis of the particle. Each particle was then interpolated with ellipse having the same normalized second central moment, as the segmented region to obtain the short and long axes in the x-y plane. These sizes are enlarged, since the tip used for the measurement has finite dimensions and thus the resulting image is a convolution of both the sample and the tip (Figure 5.4). Because of this effect the measured axes are not the real ones and the tip contribution had to be determined. The tip contribution was calculated by subtracting the z-size from the short axis of the ellipse. The long axis could thus be calculated from the enlarged long axis of the ellipses. A simplification that the tip contribution is the same in each direction (meaning the tip is a cone), was applied. The aspect ratio of the nanorods was then calculated using Formula 1.

It is possible to use the algorithm for nanorods aspect ratio determination for the diameter calculation of spherical nanoparticles as well. The aspect ratios would be close to 1 and the obtained axes sizes would correspond to the diameter.

The written programs as well as an example of their work is attached in the appendix (Appendix A, B and C respectively) of this thesis.

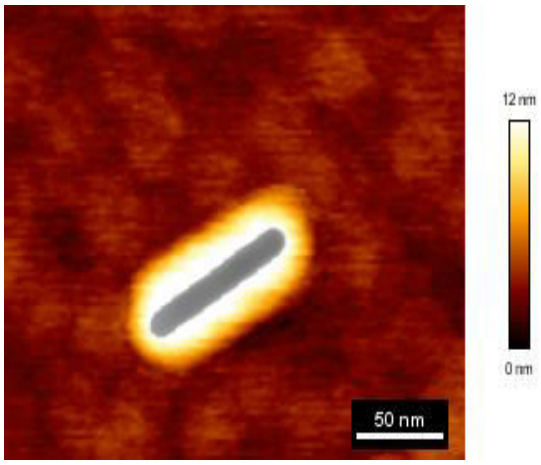

***Figure 5.4**: An illustrative example of the AFM image enlargement in comparison to TEM/SEM images (grey image on top of the AFM image) due to cantilever convolution.*

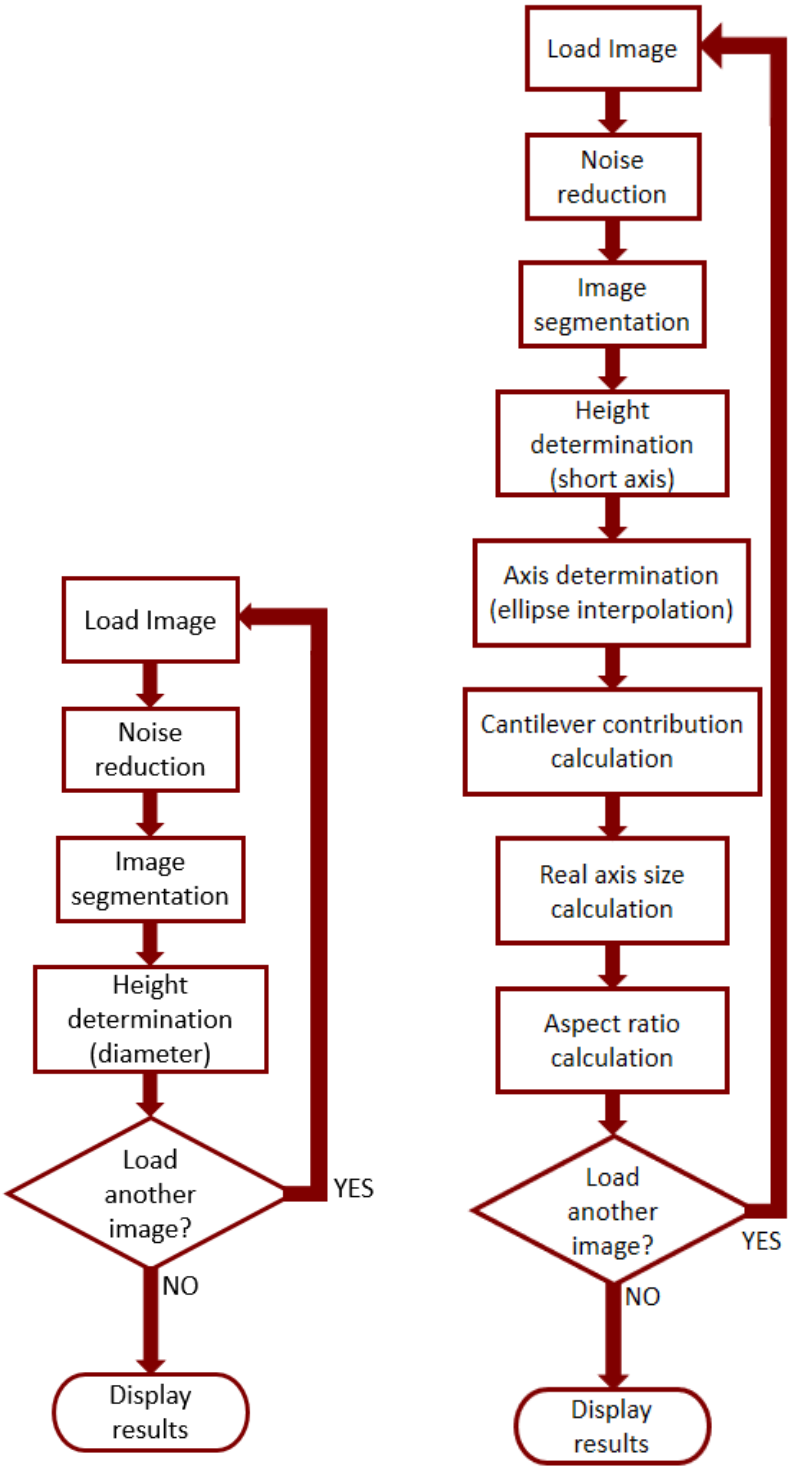

Figure 5.5: *Program algorithms for the image analysis of the results obtained from AFM. Left is the algorithm for the calculation of diameter of spherical nanoparticles. Right is algorithm for the calculation of aspect ratio of nanorods.*

5.3. SPHERICAL NANOPARTICLES

AFM, DLS and other methods have been previously compared using spherical nanoparticles. Thus, the first step of this work, was to compare both methods in the means of determining the size of two different spherical nanoparticles.

The results can be seen below. First, the control images are presented in Figure 5.6. The former showing the bigger AgNP and the latter smaller AuNP Because of the better graphics, for small nanoparticles, TEM images were used instead of SEM Following, the exemplary images of the nanospheres obtained from AFM measurements are shown for the AuNP and AgNP in Figure 5.7. Again, on the left are the AgNP and on the right AuNP. A collection of these was used as an input for the MATLAB program, where their diameter was calculated. More images of spherical nanoparticles are presented in Appendix D.

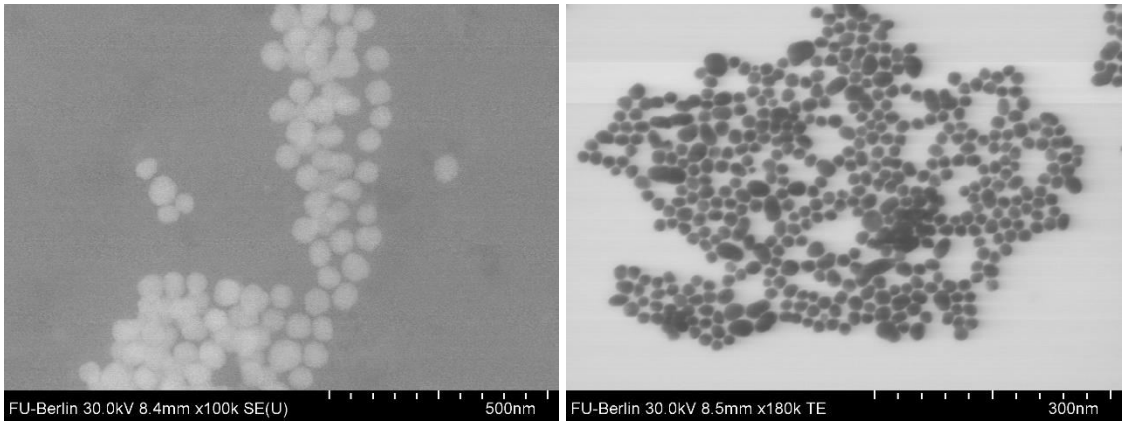

Figure 5.6: *Control images of the samples using TEM/SEM. On the left is SEM image of the bigger AgNP, on the right TEM image of the smaller AuNP.*

In Graphs 5.1 and 5.3 the results from DLS measurements are recorded. They are shown as size distribution by intensity obtained from three measurements.

In the overlapped histograms (Graphs 5.2 and 5.4) the size distributions obtained from the measurements on AFM and TEM/SEM are shown. The data from TEM/SEM were obtained from about 100 particles, whereas from AFM from about 60. Therefore, the particle numbers are normalized.

The results as diameter means ± standard deviations are shown in Table 5.1 for comparison of DLS, AFM and TEM/SEM results.

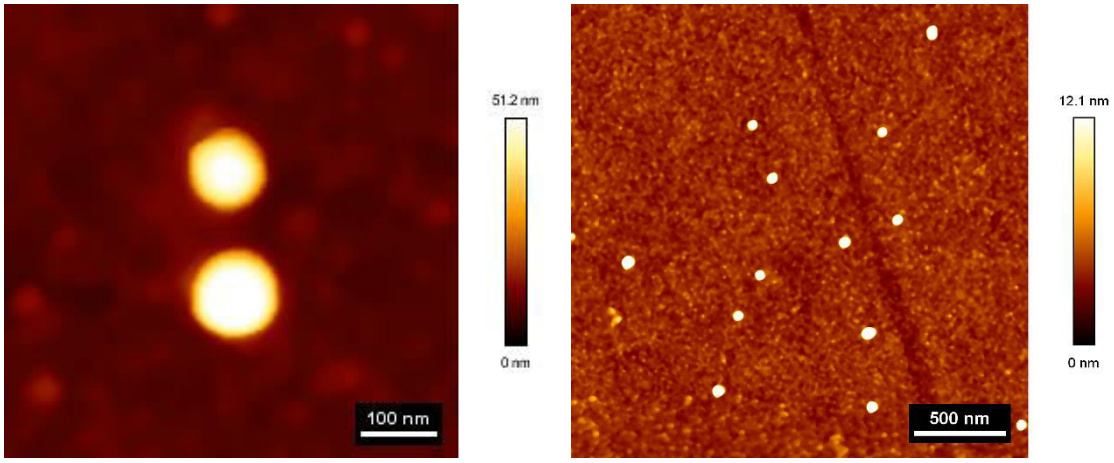

Figure 5.7: *Exemplary height images measured using AFM. Left are two AgNP, right are the smaller AuNP.*

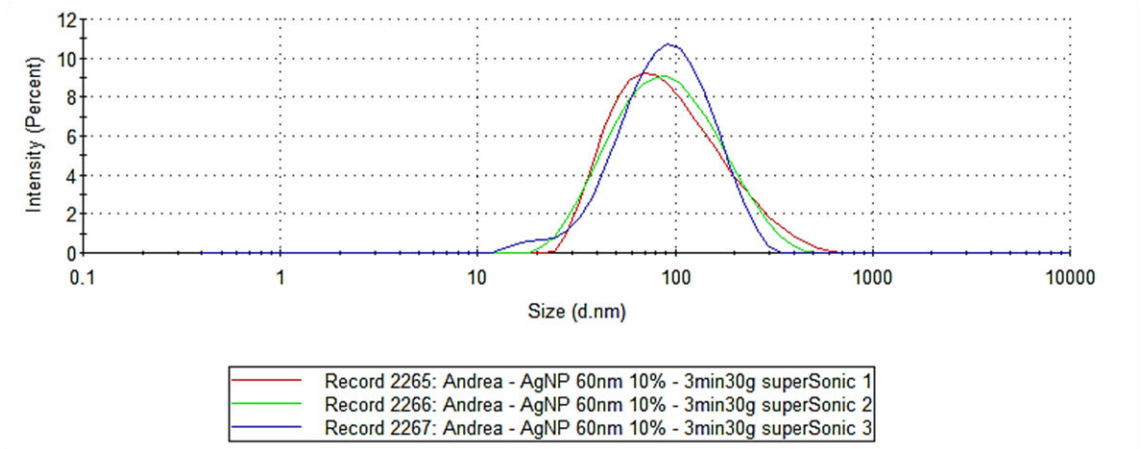

Graph 5.1: *Size distribution of the AgNP by intensity obtained from three different measurements on DLS, hence the three curves. Each curve was obtained from a measurement consisting of twelve runs.*

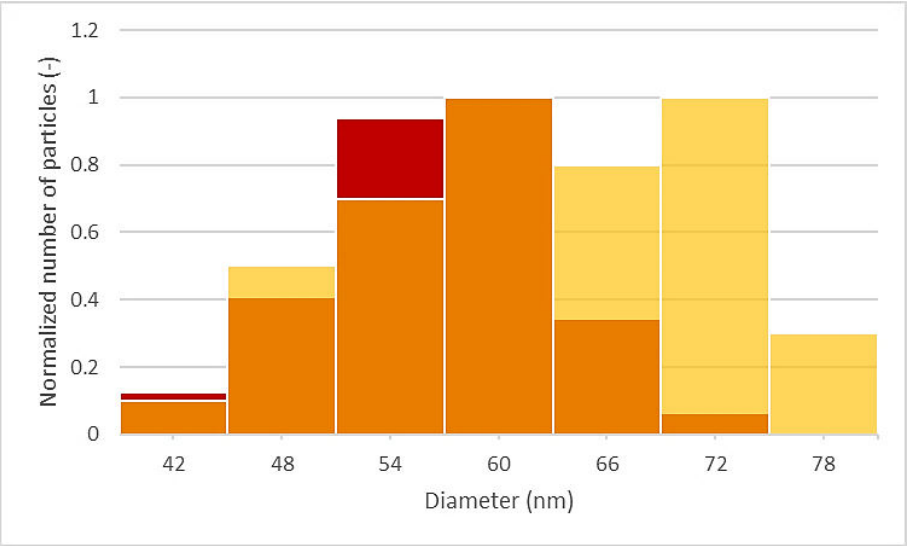

Graph 5.2: *Histograms obtained from the data of the TEM/SEM measurements (red) and AFM (yellow) for the AgNP. Orange is the region, where both histograms overlap. The number of particles is normalized.*

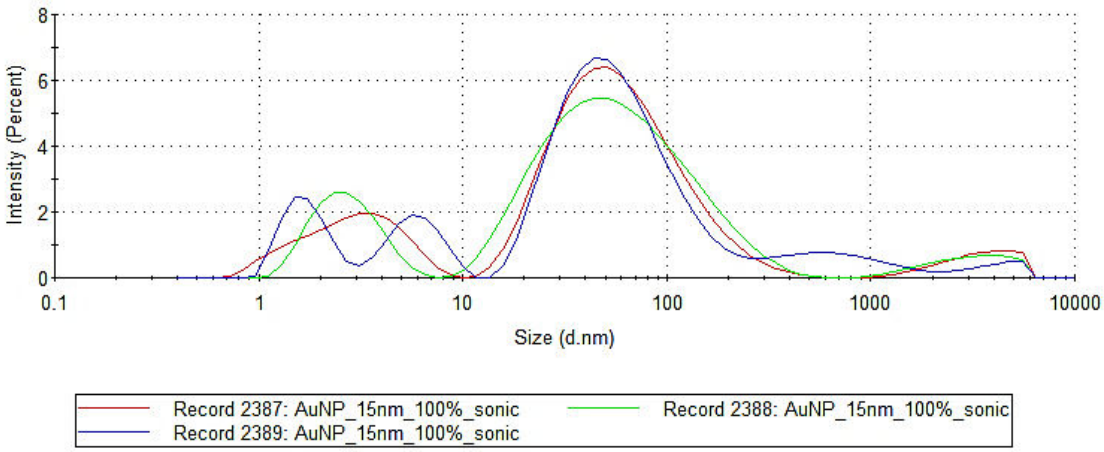

Graph 5.3: *Size distribution of the AuNP by intensity obtained from three different measurements on DLS (each curve for one measurement consisting of twelve runs). Quality issues were reported by the Zetasizer for this sample – sample is reported to be too polydisperse.*

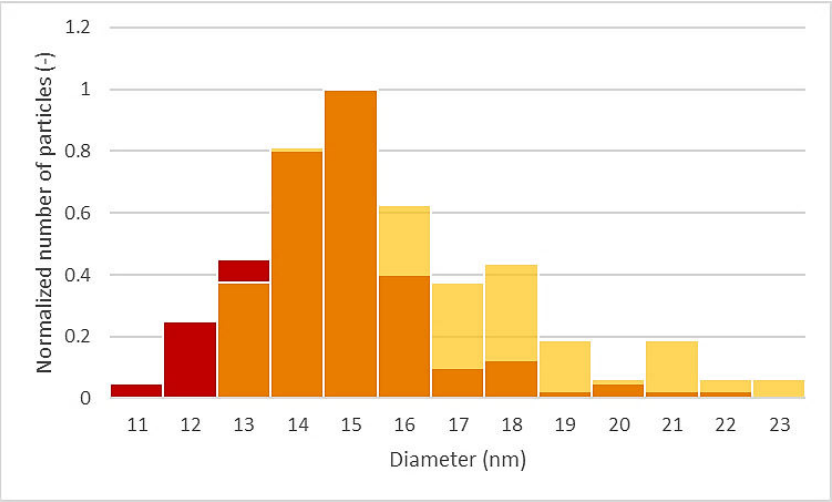

Graph 5.4: *Histograms obtained from the data of the TEM/SEM measurements (red) and AFM (yellow) for the AuNP. Orange is the region, where both histograms overlap. The number of particles is normalized.*

Table 5.1: *Summarized calculated diameters for silver and gold nanoparticles measured using TEM/SEM, AFM and DLS. The diameters are expressed as means ± standard deviations. The statistics for TEM/SEM was made from about 100 nanoparticles, for AFM from about 60 nanoparticles, DLS was calculated from three measurements, each consisting of 12 runs. Standard deviation was calculated using Formula 6.*

	TEM	**AFM**		**DLS**	
	d (nm)	d (nm)	Z-average	PdI	σ (nm)
AgNP	53.6 ± 6.5 nm	58.6 ± 8.8 nm	76.84	0.227	36.49
AuNP	14.2 ± 1.8 nm	15.5 ± 2.3 nm	-	0.828	-

According to our control results from TEM/SEM, the silver nanoparticles are about 54 nm in diameter. AFM results showed similar size distribution, slightly shifted towards bigger values. Also, the size distribution is wider, than the one obtained from TEM. DLS on the other hand showed results distinctly shifted towards the higher end of the size distributions obtained from TEM/SEM and AFM. The polydispersity index showed a value of 0.227, which indicates a polydisperse sample. The size distributions were very wide, which is also indicated by the standard deviation calculated using Formula 6.

AuNP appear to have a size of roughly 14 nm according to the control measurements from TEM/SEM. The results from AFM show similar size distribution and mean diameter. For DLS the instrument reported quality issues with the sample, as the polydispersity index is very high. Multiple peaks can be seen in all of the measurements. Therefore, the results are not available.

5.4. NANORODS

The shape of nanoparticles also greatly influences their properties and interaction. Nanorods where therefore measured, with the intend of calculating their aspect ratio.

Here, TEM images were used as a control. They yield the same accuracy as SEM images and the rods were more distinguishable (Figure 5.8). Further, exemplary images obtained from AFM are shown in Figure 5.9. More images of nanorods are presented in appendix E.

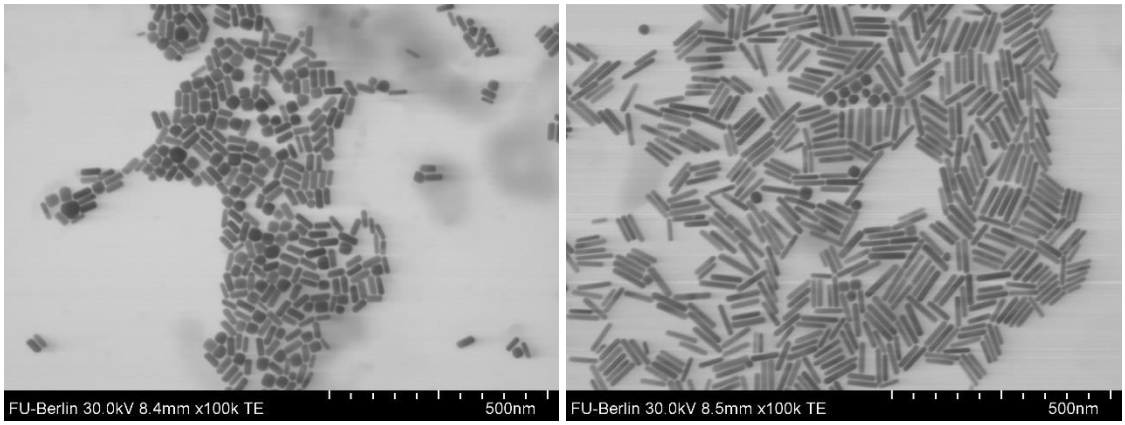

Figure 5.8: *Control images obtained from TEM/SEM for the short (left) and long (right) nanorods. The sample with short nanorods shows quite polydisperse character, since not only rods are present, but also spheres and cubes.*

The DLS results can be seen in Graphs 5.5 and 5.7, again as size distribution by intensity from three runs of measurements. For nanorods, as for small nanospheres, DLS reported quality issues with the samples. It was not possible to derive any size characteristics for the nanorods from the DLS measurements.

The overlapped histograms (Graphs 5.6 and 5.8) show size distributions for TEM/SEM and AFM. Because of the different number of particles used for the data collection (around 100 for TEM and around 60 for AFM), the values of particle numbers were normalized.

In Table 5.2 the results are summarized for the aspect ratios calculated from the images obtained from TEM/SEM and AFM.

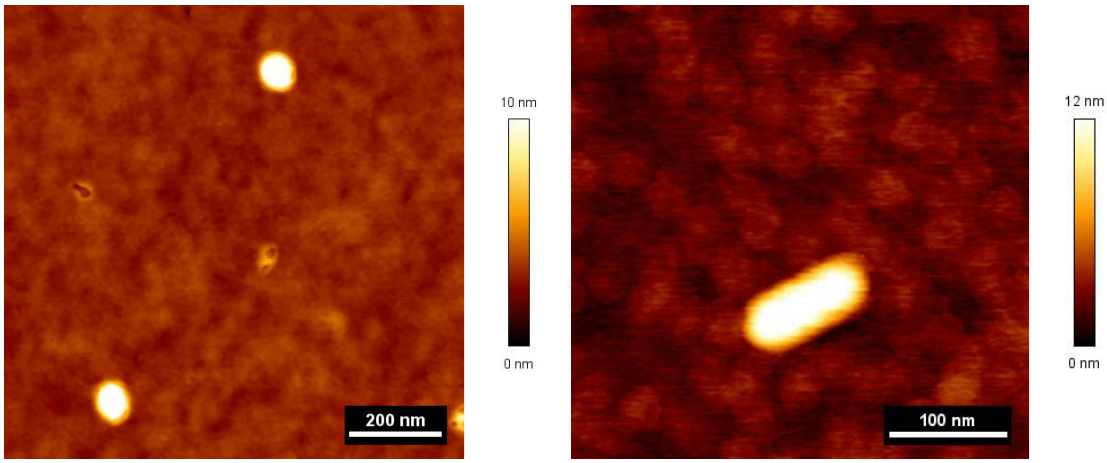

Figure 5.9 : *Exemplary images obtained from AFM for short nanorods (left) and long nanorods (right). Note that both images look enlarged in comparison to the results from TEM/SEM, because of convolution with the cantilever.*

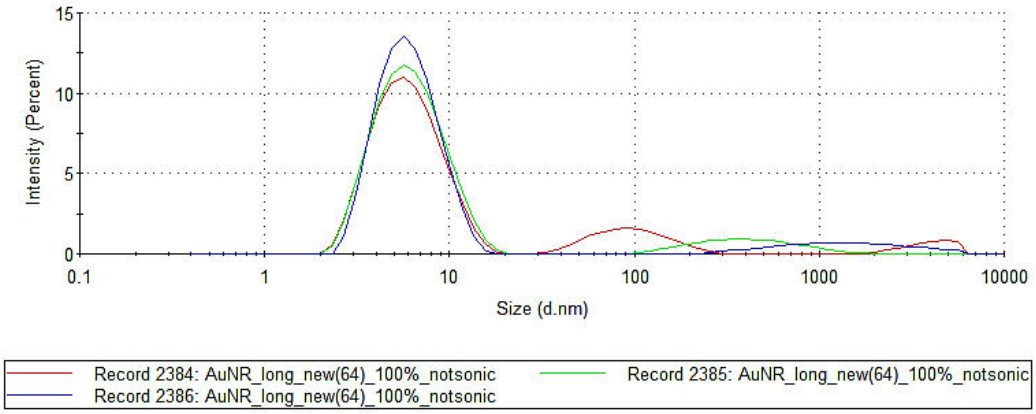

Graph 5.5*: Size distribution by intensity obtained from DLS for the long nanorods. Multiple peaks can be seen, indicating multiple detected diffusion coefficients. It is not possible to derive the nanorod size from the measured results. Graph made fused from three measurements each consisting of 12 runs.*

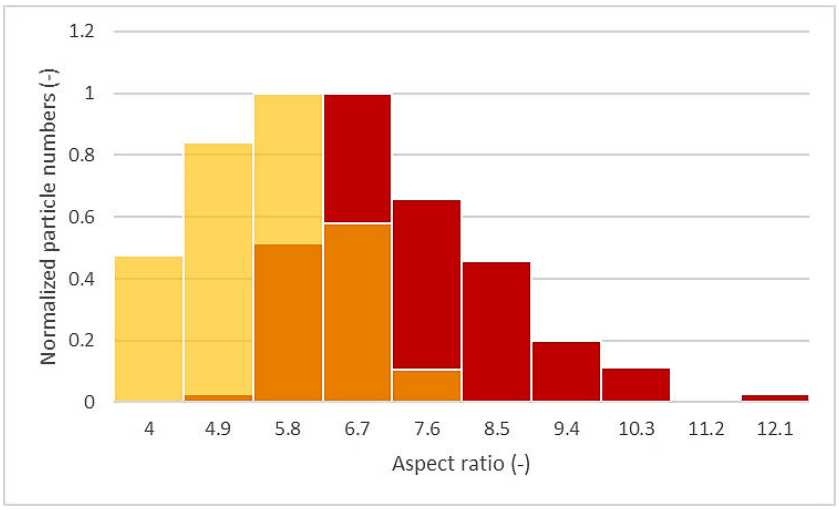

Graph 5.6: *Histograms generated for the results measured using TEM/SEM (red) and AFM (yellow), orange colour shows the overlap of both distributions. Number of particles is normalized.*

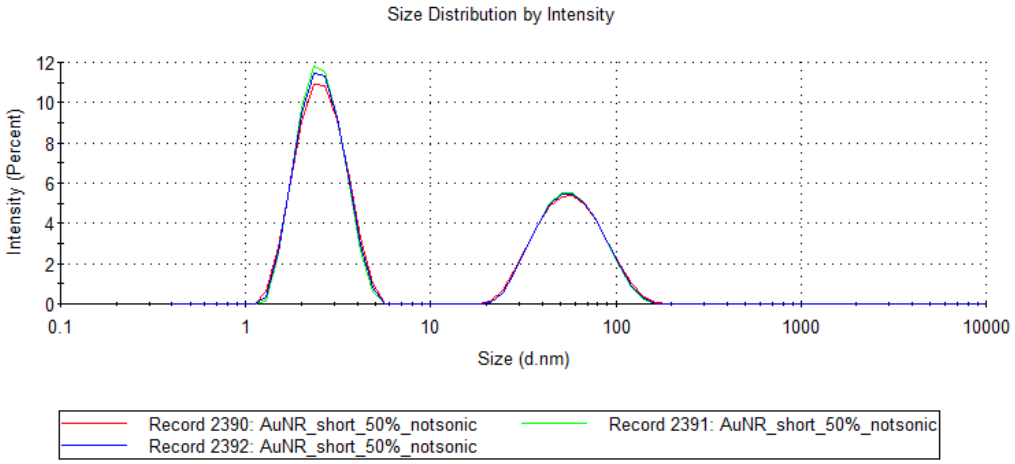

Graph 5.7: *Size distribution by intensity measured using DLS for the short nanoparticles. (each curve for one measurement consisting of twelve runs). Two distinct peaks can be seen, indicating two found diffusion coefficients. Quality issues were reported by the zetasizer – sample is reported to be too polydisperse..*

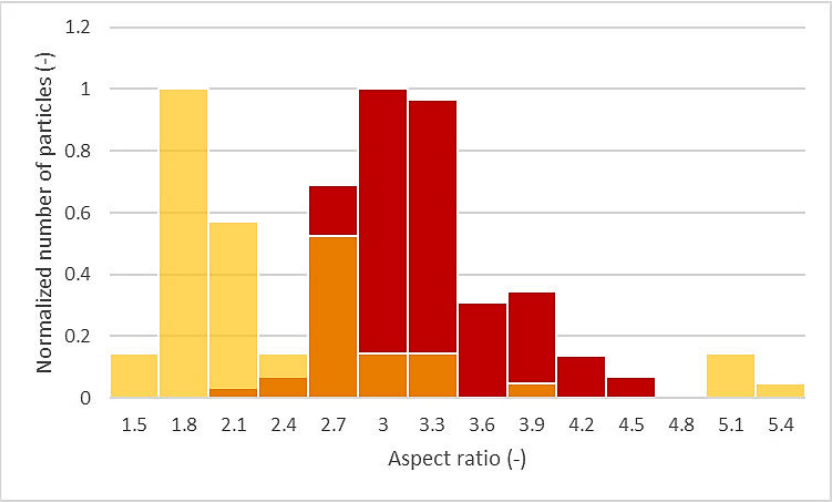

Graph 5.8: *Histograms describing the aspect ratio distribution for the short nanoparticles. Results from TEM/SEM are in red, from AFM in yellow, overlap of the two distributions is in orange. Bimodal distribution can be observed in the AFM results – one peak is around 1.8 and the other around 2.7. Number of particles is normalized.*

Table 5.2: *Summarized aspect ratio results calculated from the results from TEM/SEM and AFM. The results from DLS are not usable for the calculation of the nanorod size.*

	TEM	**AFM**	**DLS**
AuNR short	3.06 ± 0.46	2.03 ± 0.9	-
AuNR long	6.95 ± 1.33	5.01 ± 0.92	-

The control results from TEM/SEM showed that the long nanoparticles have a mean aspect ratio of about 7. The mean aspect ratio calculated from the results from AFM is lower, as well as the whole aspect ratio distribution, which is shifted towards lower values. DLS results are not applicable for the determination of the actual size of the nanorods. For long nanorods, a single distinguishable peak was recorded around 6.34 nm. Another peak is visible for each of the three measurements, however it is placed around different sizes for each one (101 nm, 475 nm or 1701 nm).

The short nanorods when measured using TEM/SEM show a mean aspect ratio of 3. Here, AFM results yielded a lower mean aspect ratio again. The aspect ratio distribution however shows

bimodal behaviour. There are two peaks visible, one around 1.8 and one around 2.7. In the case of the short nanorods, DLS showed a clear bimodal distribution with two peaks – one around 2.62 nm and one around larger sizes of 60 nm. Out of this measurement, no clear conclusion about the nanorods size can be deducted.

6. DISCUSSION

The size and shape of nanoparticles are important characteristics that influences greatly their properties. Two methods, which can be used for nanoparticle size determination, have been compared within this paper – AFM and DLS.

6.1. AFM MEASUREMENT OPTIMIZATION

In order to correctly and as precisely as possible with the given equipment measure the samples via AFM, measurement optimization was performed using a reference sample. The optimization measurements were held in air and in water using contact and non-contact mode. The best resolution for each mode and environment was attempted with the given cantilevers.

According to literature, scanning in liquid is one of the most commonly used technique when using AFM, mainly because of the extensive use of AFM in biological applications. There, the samples themselves are quite sensitive to the environment and the tendency is to keep them in their native state. Liquid measurements are also easier to reproduce. The main difference of liquid in comparison to air, is the tip-sample interactions, which are damped in liquid. [40] Also, during air measurements, a water meniscus between the sample and the tip is present, influencing the interaction and therefore the result. [66] [67]

However, as our measurements also showed, measurements in liquid (water in our case) are quite complicated in the means of preparation and measurement. Measurements in liquid are generally preferred in contact mode. There, the only drawback being the low scanning speed in our measurements. The slow speed was mainly because of oscillations of the cantilever when the speed was increased. The oscillations were probably caused by the movement of the cantilever in the x-y plane while scanning a bigger scan region. Measurements were carried both, in a liquid cell and in only a water droplet. Liquid cell was however found to be more suitable, since the water droplet moves more, because it does not have any fixed boundaries. There is also the need to add more liquid between measurements, because the droplet evaporates more easily in comparison to the liquid enclosed in the cell. [40]

When measuring in tapping mode, the first challenge to overcome is finding the right resonance frequency to drive the cantilever oscillation. In liquid, multiple peaks are present, and the resonance frequency is much lower than in air. Another limitation is that the oscillation of the

cantilever actually causes vibrations of the liquid as well, influencing the measurement. [68] These were not so present in our measurements, therefore, the measurements yielded similar results in contact and non-contact in water.

Measurements in air were quite straightforward and in general faster than the ones in liquid. As mentioned above, the main issue when measuring in air is the water meniscus forming around the tip and the sample, making it difficult to measure using small forces. This is a problem when measuring soft samples and samples not so well attached to the substrate (large forces can cause their movement). This was however not an issue during our measurement.

From our measurements we obtained images, which for each mode and environment combination showed comparable resolution. For further measurements air was chosen as the media, because of easier and faster preparation and measurement. Non-contact (tapping) mode was then chosen, since it introduces smaller forces to the sample in comparison to contact mode in air.

6.2. SPHERICAL NANOPARTICLES

Nanoparticles come in different shapes and sizes and by tuning these characteristics, the physical, optical and other properties change. Therefore, it is important to be able to correctly and as precisely as possible determine the size of the particles. The spherical shape is one of the most commonly used for metallic nanoparticles in biomedicine. [69] There, the size is determined by the particle diameter.

Nanoparticle size and shape determination is most often done using TEM or SEM techniques. They are precise and in most studies used as a control techniques. However, mostly because of their complicated measurement preparation and user unfriendly operation, other techniques are sought, which might yield comparable yet more easily achievable results. [70]

AFM, as another microscopic technique, is one of the possible techniques, which could match the TEM and SEM precision as to size and shape determination. Multiple studies have shown that AFM measurements of spherical nanoparticles yield results comparable to the ones obtained from electron microscopes. [49] [71] [72] This was also the case in our measurements. The sizes for both silver and gold spherical nanoparticles are virtually the same when calculated from each measurement. Here, the data analysis from AFM is quite straightforward. Some artefacts could alter the height image and therefore change the detected particle diameter (for example adhesion forces between the tip and the sample, or just some height changes in the substrate) [73] [74], however, these did not occur too often and are therefore not visible in the measured results.

DLS is extensively used technique mainly because of its easy operation, fast measurement, great sensitivity and analytical power. The data analysis is however quite demanding and complex. Moreover, for particle size determination, the results obtained do not match the real sizes, because of the DLS principle, where it considers a layer of solvent around the particle to be a part of it. Thus, the results from DLS are not quite precise. [72] [65] As a tool for approximate sample characterization it is sufficient. The increased particle size was also a result of our measurements. For the larger AgNP of about 50 nm, DLS showed results of the mean diameter in the higher end of the size distribution obtained by SEM/TEM. Apart from the solvation layer, another reason behind the bigger sizes is the fact that the intensity of scattered light is dependent on the sixth power of the nanoparticle size. [50] Thus, larger particles tend to cover smaller ones in the results. The distribution obtained from the DLS measurements is also quite broad. The standard deviation was calculated out of the polydispersity index. Since

the instrument reported a quite polydisperse sample (a PdI larger than 0.1), the distribution is broadened and therefore the standard deviation is so big.

The smaller AuNP of about 15 nm were a more demanding sample, which was not possible to measure using the given instrument. The instrument reports a detection limit of about 0.3 nm, which is much smaller that the nanoparticles measured. Therefore, the probability that the particles were just too small for the detector, is not very high. Another possibility could be that there were aggregations and impurities, causing the increased polydispersity reported by the instrument.

6.3. NANORODS

Along with the synthesis of spherical nanoparticles, numerous different shapes also emerged. The various shapes offer more diversity as to properties and characteristics of the nanoparticles. [75] As with spherical nanoparticles, the properties of the differently shaped particles change with the size. [76] This study focused, apart from spherical nanoparticles, on nanorods and their size characterization.

Two different samples were observed, one with long nanorods and one polydisperse with a combination of short nanorods, cubes and spheres. Both were measured using TEM/SEM as a control.

DLS is in essence a method, which determines the characteristics of a sphere with the same hydrodynamic properties, as the sample used. Thus, is it primarily used for determining the size of spherical nanoparticles. When rod-like nanoparticles are measured, DLS should show a distinguishable result. The resulting size by intensity graph should have two peaks, each one representing a diffusion coefficient. Because of the non-symmetrical shape, there are contributions to the overall hydrodynamic behaviour of the rods. One is the conventional translational coefficient, which in spherical nanoparticles can be used for the determination of the diameter the second is the rotational diffusion coefficient. [77] A study has shown that the higher the aspect ratio of gold nanoparticles, the higher is the first peak in the DLS measurements, which corresponds to the rotational diffusion coefficient. [52]

The obtained DLS results for long AuNR showed one large peak and for each measurement another smaller peak at a different position in the distribution. The two peaks could be expected, however no clear deduction as for the nanorods size (more precisely aspect ratio) can be concluded because of the non-consistent results.

For the short nanorods, the size distribution by intensity shows a clear bimodal course. The first peak can be assigned to the rotational diffusion coefficient, and its height increases with the increasing aspect ratio. When compared to another study done for gold nanorods and their size determination using DLS ([52]), the resulting size distribution by intensity look quite similar. This comparison is however not applicable, because of different measurement conditions and equipment used. An aspect ratio determination could probably be done, if multiple samples of different nanorods of known aspect ratios were measured as reference. This method is however utilizable only for samples, where it is known that they are of nanorods (and what kind of

nanorods). In unknown samples, it would not be clear, if there are rods or polydisperse samples of spheres.

Another problem with the short nanorods, which influences the DLS measurements, is the fact that one of their absorption peak is overlapping with the wavelength used for the DLS (see Appendix F for the graph of absorbance of the nanoparticles used in this work). The results can therefore not be safely used. This could have a connection to the fact that DLS reported quality issues for the samples with short nanorods. Another phenomenon influencing the resulting size distribution is the sample polydispersity, which can be seen in the TEM/SEM images. This polydispersity was also one of the reasons behind the report from the DLS instrument.

The results from AFM in both cases show a lower aspect ratio, than the results from SEM/TEM. This is probably caused by the fact that during the image analysis a simplification was used, where the tip was considered a cone, which means that the contribution of the tip is the same in every direction. The tip is, however, not a perfect cone, rather a rotated monolith, slightly tilted. Another reason behind the lower aspect ratios could be that during data analysis, some data were lost because of the automatic evaluation and the automatic interpolation with ellipses. The latter could be solved by manually choosing the axes, from which the real sizes are calculated. This however would enormously extend the analysis time.

Another aspect, which could be behind the lower aspect ratios, is the difference in adhesion at the sample and substrate. This would lead to height anomalies during the measurement. [73] This effect was not observable, when measuring spherical nanoparticles, however with the rod-like particles, the glass substrate was covered in CTAB, which was used as a surfactant in the sample and was not thoroughly washed. The CTAB-tip interaction is different than glass-tip and the adhesion difference changes the experienced force by the tip and therefore the measured height. [78]

As can be seen in the Figure 5.8 from TEM/SEM, the sample with short nanorods is quite polydisperse, as there are not only rods, but also spheres and cubes. These were not included in the data analysis from TEM/SEM (the aspect ratio distribution is solely calculated from the sizes of nanorods). The data from AFM however showed a bimodal aspect ratio distribution. One of the peaks being around 1.8 and the other around 2.7. This implies the fact that the sample is polydisperse, with two types of nanorods – with higher and lower aspect ratio. The lower one is from the particles that were closer to the spherical ones. The higher aspect ratios belong to the nanorods as they were reported from TEM/SEM. The obtained aspect ratio for the nanorods

(2.7) is again smaller, than the one calculated from TEM/SEM, the same probable causes as with longer nanorods can be assumed.

The results from the short polydisperse nanorods show that AFM could be utilizable as a polydispersity determiner. This has already been shown in other studies, where AFM was used for the measurements of polydisperse samples. When used for spherical nanoparticles, AFM yielded bimodal distributions for the diameter. [49] Here, we presented a bimodal distribution of aspect ratios, polydisperse samples of nanorods are therefore also measurable. The main problem with AFM and polydispersity characterization, is the need of many images for statistical processing.

7. CONCLUSION

Nanoparticles are a promising new material with plethora of different uses in multiple fields including biomedicine. Their unique properties derive from their size and shape and therefore, there is the need to determine those as precisely as possible. This could offer not only feedback during synthesis, but also help predict their properties before use. Multiple methods can be used, in this work, AFM and DLS were compared for the determination of the diameter of spherical nanoparticles, aspect ratio of nanorods and characteristics of a polydisperse sample.

An image analysis program was programmed for the data interpretation from AFM for both spherical and rod-like nanoparticles.

Our results showed that both AFM and DLS, are comparable to the control method – TEM/SEM, when measuring spherical nanoparticles. DLS showed results higher, than those obtained from TEM/SEM, due to the very nature of the technique, which measures the hydrodynamic diameter, rather than the real one. The results from AFM were much closer to the ones obtained from TEM/SEM.

As for nanorods, DLS is not a method, which could determine the size directly. A reference measurement could be used, however, this is not applicable for unknown samples. AFM images and their analysis showed results similar to the ones obtained from TEM/SEM. The calculated aspect ratios are shifted towards the lower end of the aspect ratio distribution. These discrepancies could be caused by either errors during image analysis, or anomalies arising from the tip-sample interactions.

A polydisperse sample of nanorods was measured as well. AFM showed an ability to determine the bimodal distribution, therefore a polydispersity analysis can be obtained when measuring with AFM. However, for statistical interpretation, a lot of images are needed, which increases the measurement time. DLS is quite sensitive to polydispersity, however no usable result as to the characteristic of the particles could be obtained.

Overall, the main advantages of DLS are the fast measurement time and easy operation, the data analysis is on the other hand quite demanding. AFM measurement time is much longer, the results were however more precise. In comparison to TEM/SEM, AFM has another advantage, which is its easy use in biological measurements.

8. REFERENCE

[1] S. Horikoshi a N. Serpone, „Introduction to Nanoparticles," v *Microwaves in Nanoparticle Synthesis*, Weinheim, Wiley-VCH Verlag GmbH & Co. KGaA,, 213, pp. 1-24.

[2] „National Nanotechnology Initiative," [Online]. Available: https://www.nano.gov/nanotech-101/special. [Přístup získán 8 May 2017].

[3] A. Albanese a e. al., „The Effect of Nanoparticle Size, Shape, and Surface Chemistry on Biological Systems," *Annual Review of Biomedical Engineering,* pp. 14:1-16, 2012.

[4] O. Salata, „Applications of nanoparticles in biology and medicine," *Journal of nanobiotechnology,* p. 2:3, 2004.

[5] W. e. a. Jiang, „Nanoparticle-mediated cellular response is size-dependent," *Nature Nanotechnology,* sv. 3, pp. 145-150, 2008.

[6] S. E. A. e. a. Gratton, „The effect of particle design on cellular internalization pathways," *PNAS,* sv. 105, p. 11613–18, 2008.

[7] Y. e. a. Qiu, „Surface chemistry and aspect ratio mediated cellular uptake of Au nanorods," *Biomaterials,* sv. 31, č. 30, pp. 7606-7619, 2010.

[8] M. e. a. Neshatian, „Determining the Size Dependence of Colloidal Gold Nanoparticle Uptake in a Tumor-like Interface (Hypoxic)," *Colloids and Interface Science Communications,* sv. 1, pp. 57-61, 2014.

[9] H. e. a. Gao, „Mechanics of receptor-mediated endocytosis," *PNAS,* sv. 102, č. 27, pp. 9469-74, 2005.

[10] P. Decuzzi a M. Ferrari, „The Receptor-Mediated Endocytosis of Nonspherical Particles," *Biophysical Journal ,* sv. 94, č. 10, p. 3790–3797, 2008.

[11] M. Slevin, „Current Advance in the Medical Application of Nanotechnology," Bentham Press, 2012.

[12] Geng a Y. e. al., „Shape effects of filaments versus spherical particles in flow and drug delivery," *Nature Nanotechnology ,* sv. 2, pp. 249-255, 2007.

[13] H. S. e. a. Choi, „Renal clearance of quantum dots," *Nature Biotechnology,* sv. 25, pp. 1165-1170, 2007.

[14] H. C. Fischer a e. al., „Pharmacokinetics of nanoscale quantum dots: In vivo distribution, sequestration, and clearance in the rat.," *Advanced functional materials,* sv. 16, č. 10, pp. 1299-1305, 2006.

[15] G. e. a. Sonavane, „Biodistribution of colloidal gold nanoparticles after intravenous administration: Effect of particle size," *Colloids and Surfaces B: Biointerfaces,* sv. 66, č. 2, pp. 274-280, 2008.

[16] L. A. Dykman a N. Khlebtsov, „Gold Nanoparticles in Biology and Medicine: Recent Advances and Prospects," *Acta Naturae,* sv. 3, č. 2, pp. 34-55, 2011.

[17] C. Noguez, „Surface Plasmons on Metal Nanoparticles: The Influence of Shape and Physical Environment," *Journal of Physical Chemistry,* sv. 111, pp. 3806-3819, 2007.

[18] A. M. Alkilany a C. J. Murphy, „Toxicity and cellular uptake of gold nanoparticles: what we have learned so far?," *Journal of nanoparticle research,* pp. 2313-2333, 2010.

[19] V. e. a. Amendola, „Physico-Chemical Characteristics of Gold Nanoparticles," *Comprehensive Analytical Chemistry,* sv. 66, pp. 81-152, 2014.

[20] S. Lee a X. Chen, „Activavable Optical Probes for Cancer Imaging," v *Molecular Imaging Probes for Cancer Research*, Singapore, World Scientific Publishing Co. Pte. Ltd., 2012, pp. 531-535.

[21] L. R. e. a. Hirsch, „Nanoshell-mediated near-infrared thermal therapy of tumors under magnetic resonance guidance.," *PNAS,* sv. 100, č. 23, pp. 13549-54, 2003.

[22] X. Huang a M. A. El-Sayed, „Gold nanoparticles: Optical properties and implementations in cancer diagnosis and photothermal therapy," *Journal of Advanced Research,* pp. 13-28, 2010.

[23] C. S. e. a. Kim, „Cellular imaging of endosome entrapped small gold nanoparticles," *MethodsX,* sv. 2, pp. 306-315, 2015.

[24] Y. H. e. a. Chen, „Methotrexate conjugated to gold nanoparticles inhibits tumor growth in a syngeneic lung tumor model.," *Molecular Pharmaceutics,* sv. 4, č. 5, pp. 713-22, 2006.

[25] O. A. e. a. Swiech, „Doxorubicin carriers based on Au nanoparticles – effect of shape and gold-drug linker on the carrier toxicity and therapeutic performance," *RSC Advances,* sv. 6, pp. 31960-67, 2016.

[26] V. e. a. Juve, „Size-Dependent Surface Plasmon Resonance Broadening in Nonspherical Nanoparticles: Single Gold Nanorods," *Nano Letters,* sv. 13, č. 5, pp. 2234-2240, 2013.

[27] H. e. a. Huang, „Optical and biological sensing capabilities of Au2S/AuAgS coated gold nanorods," *Biomaterials,* sv. 30, č. 29, pp. 5622-5630, 2009.

[28] M. S. e. a. Khan, „Highly efficient gold nanorods assisted laser phototherapy for rapid treatment on mice wound infected by pathogenic bacteria," *Journal of Industrial and Engineering Chemistry,* sv. 36, č. 25, pp. 49-58, 2016.

[29] Z. e. a. Li, „Metabolizable Small Gold Nanorods: Size-dependent Cytotoxicity, Cell Uptake and In Vivo Biodistribution," *ACS Biomaterials Science and Engineering,* sv. 2, č. 5, pp. 789-797, 2016.

[30] Q. H. e. a. Tran, „Silver nanoparticles: synthesis, properties, toxicology, applications and perspectives," *Advances in Natural Sciences: Nanoscience and Nanotechnology, Volume 4, Number 3 ,* sv. 4, č. 3, 2013.

[31] C. A. e. a. Dos Santos, „Silver Nanoparticles: Therapeutical Uses, Toxicity, and Safety Issues," *Journal of Pharmaceutical Sciences,* sv. 103, č. 7, pp. 1931-1944, 2014.

[32] A. H. e. a. Alshehri, „Enhanced Electrical Conductivity of Silver Nanoparticles for High Frequency Electronic Applications,“ *ACS Applied Materials and Interfaces,* sv. 4, č. 12, pp. 7007-7010, 2012.

[33] X. e. a. Hua, „Photonic crystals with silver nanowires as a near-infrared superlens,“ *Applied Physics Letters,* sv. 85, č. 9, pp. 1520-23, 2004.

[34] M. A. e. a. Franco-Molina, „Antitumor activity of colloidal silver on MCF-7 human breast cancer cells,“ *Journal of Experimental & Clinical Cancer Research,* sv. 29, p. 148, 2010.

[35] A. e. a. Jillavenkatesa, Particle Size Characterization, Washington: U.S. Government Printing Office, 2001.

[36] P. A. Webb a C. Orr, „Modern Methods of Particle Characterization, Part 1: Particle Size,“ *American Ceramic Society Bulletin,* sv. 85, č. 5, pp. 25-28, 2006.

[37] R. Egerton, Physical Principles of Electron Microscopy, Edmonton: Springer Science+Business Media, Inc., 2005.

[38] B. Hafner, „Scanning Electron Microscopy Primer,“ 16 04 2007. [Online]. Available: http://www.charfac.umn.edu/sem_primer.pdf. [Přístup získán 8 May 2017].

[39] D. A. Muller a J. Grazul, „Optimizing the environment for sub-0.2 nm scanning transmission electron microscopy,“ *Journal of Electron Microscopy ,* sv. 50, č. 3, pp. 219-226, 2001.

[40] P. Eaton a P. West, Atomic Force Microscopy, New York: Oxford University Press, 2010.

[41] V. Bellitto, Atomic Force Microscopy - Imaging, Measuring and Manipulating Surfaces at the Atomic Scale, Rijeka: InTech, 2012.

[42] O. e. a. Custance, „Atomic force microscopy as a tool for atom manipulation,“ *Nature Nanotechnology,* sv. 4, pp. 803-810, 2009.

[43] F. A. e. a. Ferri, „Magnetic Force Microscopy: Basic Principles and Applications,“ v *Atomic Force Microscopy - Imaging, Measuring and Manipulating Surfaces at the Atomic Scale*, Rijeka, InTech, 2012, pp. 39-56.

[44] S. Xu, „Some Basic Principles of AFM Sample Preparation,“ [Online]. Available: https://www.agilent.com/cs/library/slidepresentation/Public/Some%20Basic%20Principles%20Sample%20Preparation_Song%20Xu_032708.pdf. [Přístup získán 8 May 2017].

[45] J. Instruments, „NanoWizard 3 User Manual,“ 09 2012. [Online]. Available: http://www.nanophys.kth.se/nanophys/facilities/nfl/afm/jpk/manuf-manuals/usermanual.4.2.pdf. [Přístup získán 8 May 2017].

[46] P. Klapetek, D. Nečas a C. Anderson, „Gwyddion user guide: Tip Convolution Artefacts,“ 2003. [Online]. Available: http://gwyddion.net/documentation/user-guide-en/tip-convolution-artefacts.html. [Přístup získán 8 May 2017].

[47] B. J. Berne a R. Pecora, Dynamic Light Scattering, Toronto: General Publishing Company, Ltd., 2000.

[48] L. Kvítek, „Učební test: Metody studia koloidních soustav,“ 2006. [Online]. Available: http://chemikalie.upol.cz/skripta/msk/msk.pdf. [Přístup získán 8 May 2017].

[49] C. M. Hoo a e. al., „A comparison of atomic force microscopy (AFM) and dynamic light scattering (DLS) methods to characterize nanoparticle size distributions,“ *Journal of Nanoparticle Research,* č. 10, pp. 89-96, 2008.

[50] nanoComposix, „NanoComposix's Guide to Dynamic Light Scattering Measurement and Analysis,“ February 2015. [Online]. Available: https://cdn.shopify.com/s/files/1/0257/8237/files/nanoComposix_Guidelines_for_DLS_Measurements_and_Analysis.pdf. [Přístup získán 8 May 2017].

[51] J. Rodríguez-Fernández and e. al., “Dynamic Light Scattering of Short Au Rods with Low Aspect Ratios,” *Journal of Physical Chemistry,* vol. 111, no. 13, pp. 5020-5025, 2007.

[52] H. e. a. Liu, „Dynamic light scattering for gold nanorod size characterization and study of nanorod–protein interactions,“ *Gold Bulletin,* sv. 45, č. 4, pp. 187-195, 2012.

[53] E. Tomaszewska a e. al., „Detection Limits of DLS and UV-Vis Spectroscopy in Characterization of Polydisperse Nanoparticles Colloids,“ *Journal of Nanomaterials,* 2013.

[54] G. A. Dorofeev a e. al., „Determination of Nanoparticle Sizes by X-ray Diffraction,“ *Colloid Journal,* sv. 74, č. 6, pp. 675-685, 2012.

[55] R. P. e. a. Carney, „Determination of nanoparticle size distribution together with density or molecular weight by 2D analytical ultracentrifugation,“ *Nature Communications,* sv. 2, p. 335, 2011.

[56] J. Zhang a D. Chen, „Differential Mobility Particle Sizers for Nanoparticle Characterization,“ *Journal of Nanotechnology in Engineering and Medicine,* sv. 5, č. 2, 2014.

[57] R. C. Gonzales a R. E. Woods, Digital Image Processing, New Jersey: Prentice Hall, 2002.

[58] R. e. a. Fisher, „Gaussian Smoothing,“ 2003. [Online]. Available: http://homepages.inf.ed.ac.uk/rbf/HIPR2/gsmooth.htm. [Přístup získán 8 May 2017].

[59] R. e. a. Fisher, „Median Filter,“ 2003. [Online]. Available: Median Filter. [Přístup získán 8 May 2017].

[60] L. Chun Lin, „A Tutorial to the Wavelet Transform,“ 23 February 2010. [Online]. Available: http://disp.ee.ntu.edu.tw/tutorial/WaveletTutorial.pdf. [Přístup získán 8 May 2017].

[61] G. Ramponi, „Morphological Image Processing,“ 2002. [Online]. Available: http://www2.units.it/carrato/didatt/EI_web/slides/Ch_09.pdf. [Přístup získán 8 May 2017].

[62] M. Sonka, V. Hlavac a R. Boyle, Image Processing, Analysis and Machine Vision, CL Engineering, 2014.

[63] Z. Zhang, „K-means Algorithm,“ 22 March 2012. [Online]. Available: http://user.engineering.uiowa.edu/~ie_155/lecture/K-means.pdf. [Přístup získán 8 May 2017].

[64] D. e. a. Chicea, „Assesing Fe3O4 nanoparticle size by DLS, XRD and AFM,“ *Journal of optoelectronics and advanced materials,* sv. 14, pp. 460-466, 2012.

[65] A. Bootz a e. al., „Comparison of scanning electron microscopy, dynamic light scattering and analytical ultracentrifugation for the sizing of poly(butyl cyanoacrylate) nanoparticles,“ *European Journal of Pharmaceutics and Biopharmaceutics,* sv. 57, pp. 369-375, 2004.

[66] C. Martin a F. Pérez-Murano, „Measurements of Electrical Conductivity of a Nanometer-Scale Water Meniscus by Atomic Force Microscopy,“ v *Third IEEE Conference on Nanotechnology, Vols One and Two, Proceedings*, 2003.

[67] H.-Q. Li, „The Common AFM Modes,“ 24 April 1997. [Online]. Available: http://www.chembio.uoguelph.ca/educmat/chm729/afm/details.htm. [Přístup získán 8 May 2017].

[68] T. E. e. a. Schäffer, „Studies of vibrating atomic force microscope cantilevers in liquid,“ *Journal of Applied Physics,* sv. 80, p. 3622, 1996.

[69] G. Goodrich, „Synthesis and Surface Modification of Nanomaterials for Tumor Targeting,“ v *Cancer Nanotechnology: Principles and Applications in Radiation Oncology*, Boca Raton, CRC Press, 2013, pp. 39-48.

[70] J. B. Malherbe a O. Quintin, „Bombardment-induced topography on semiconductor surfaces,“ v *Fundamental and Applied Aspects of Modern Physics*, Singapore, World Scientific Publishing Co. Pte. Ltd., 2000, pp. 201-210.

[71] A. e. a. Delvallée, „Comparison of nanoparticle diameter measurements by Atomic Force Microscopy and Scanning Electron Microscopy,“ v *16th International Congress of Metrology*, Paris, 2013.

[72] R. F. e. a. Domingos, „Characterizing Manufactured Nanoparticles in the Environment: Mutlimethod Determination of Particle Sizes,“ *Environmental Science and Technology,* sv. 43, č. 19, pp. 7277-84, 2009.

[73] S. J. T. e. a. Van Noort, „Height anomalies in tapping mode atomic force microscopy in air caused by adhesion,“ *Ultramicroscopy,* sv. 69, pp. 117-127, 1997.

[74] Á. e. a. Mechler, „Anomalies in nanostructure size measurements by AFM,“ *Physical review,* sv. 72, č. 12, 2005.

[75] A. R. M. e. a. Nabiul Afrooz, „Spheres vs. rods: The shape of gold nanoparticles influences aggregation and deposition behavior,“ *Chemosphere,* sv. 91, pp. 93-98, 2013.

[76] R. e. a. Krahne, Physical Properties of Nanorods, Berlin: Springer-Verlag, 2013.

[77] D. e. a. Lehner, „Determination of the Translational and Rotational Diffusion Coefficients of Rodlike Particles Using Depolarized Dynamic Light Scattering,“ *Langmuir,* sv. 16, pp. 1689-1695, 2000.

[78] J. H. e. a. Hoh, „Tip-sample interactions in atomic force microscopy: I. Modulating adhesion between silicon glass,“ *Nanotechnology,* sv. 2, č. 3, pp. 119-122, 1991.

APPENDIX A: MATLAB IMAGE ANALYSIS PROGRAM FOR NANOSPHERES

```
clear all;
close all;
clc;

prompt = 'Load an image?';
loop = input(prompt, 's');
Diameter = [];
%% Load Image
% Image only manipulated with polynomial fit and histogram line fit in JPK
% processing program
while loop == 'yes'
 [filename, pathname, filterindex] = uigetfile( ...
   {'*.txt','asci (*.txt)'; ...
   '*.*',  'All Files (*.*)'}, ...
   'Pick a file');
cd (pathname)
ind=length(filename);
 pat = '.txt';
    namex=regexprep(filename, pat, '');
    name=regexprep(namex, ' ', '');
    FILENAME=filename;
    NAME=name;
   fida=fopen(filename);
   HLAVA=textscan(fida,'%s',124);
   hlavicka=HLAVA{1,1};
   fclose(fida);
   fastSize=str2double(hlavicka(39));
   slowSize=str2double(hlavicka(42));
   Offset=[str2double(hlavicka(45)) str2double(hlavicka(48))];
   ij=[str2double(hlavicka(51)) str2double(hlavicka(54))];
   scanRate=str2double(hlavicka(63));
   dutcycle=str2double(hlavicka(66));
   delay=str2double(hlavicka(69));
   refAmp=str2double(hlavicka(78));
   sineAmp=str2double(hlavicka(81));
   sineFreq=str2double(hlavicka(84));
   sinePhaseShift=str2double(hlavicka(87));
   iGain=str2double(hlavicka(90));
   pGain=str2double(hlavicka(93));
   setpoint=str2double(hlavicka(105));
   dilekx=slowSize/ij(2);
   dileky=fastSize/ij(2);
   X=[dilekx:dilekx:slowSize];
   Y=[dileky:dileky:fastSize];
%     ind=length(filename);
    fid=fopen (filename);
%     HLAVA=textscan(fid,'%s',6);
%     IJa=textscan(fid,'%s',6,'HeaderLines',9);
%     IJ=IJa{1,1};
%     ij=[str2double(IJ{3}),str2double(IJ{6})];

    DAT=textscan(fid,'%n','HeaderLines',34);
    DATa = DAT{1,1,:};
%      A(1:ij(1),1:ij(2))=DATa(((1:ij(2))-1)*ij(1)+(1:ij(2)));
       for j=1:ij(2)
          for i=1:ij(1)
          HEIGHT(i,j)=DATa((i-1)*ij(2)+j);
```

```
        end
    end
%    fclose(fid);
%    surf(X,Y,HEIGHT)
%    shading interp
%    colormap (pink(128))

%% Data Analysis
% vector to matrix
Image = vec2mat(DATa, i);
ImageNorm = Image./max(max(Image));
ImageCrop = imcrop(ImageNorm);
ImageCropNorm = ImageCrop./max(max(ImageCrop));

% image to bw
ImageBW = im2bw(ImageCropNorm);

% artefacts and noise reduction
se = strel('disk', 1);
ImageOpen = imopen(ImageBW, se);
ImageClose = imclose(ImageOpen, se);
imshow(ImageClose);

% segment labelling
ImageSeg = bwlabel(ImageClose);

Diameter = [Diameter, zeros(1, max(max(ImageSeg)))];
[r, c] = size(ImageSeg);
run = 1;

for D = (length(Diameter) - (max(max(ImageSeg))-1)):length(Diameter)
    x = [];
    for R = 1:r
        for C= 1:c
            if ImageSeg(R, C) == run
            x = [x, ImageCrop(R, C)];
            end
        end
    end
    run = run+1;
    Diameter(D) = max(x)*max(max(Image));
end

prompt = 'Load an image?';
loop = input(prompt, 's');

  if isequal(loop, 'no')
    break
  end
end

Mean = mean(Diameter);
StDev = std(Diameter);
X = ['Nanoparticle size is ', num2str(Mean), ' +- ', num2str(StDev)];
  disp(X);
```

APPENDIX B: MATLAB IMAGE ANALYSIS PROGRAM FOR NANORODS

```
clear all;
close all;
clc;

prompt = 'Load an image?';
loop = input(prompt, 's');
Short = [];
ShortTemp = [];
Long = [];

while loop == 'yes'
%% Load Image
% Image only manipulated with polynomial fit and histogram line fit in JPK
% processing program
[filename, pathname, filterindex] = uigetfile( ...
   {'*.txt','asci (*.txt)'; ...
   '*.*',  'All Files (*.*)'}, ...
   'Pick a file');
cd (pathname)
ind=length(filename);
 pat = '.txt';
    namex=regexprep(filename, pat, '');
    name=regexprep(namex, ' ', '');
    FILENAME=filename;
    NAME=name;
   fida=fopen(filename);
   HLAVA=textscan(fida,'%s',124);
   hlavicka=HLAVA{1,1};
   fclose(fida);
   fastSize=str2double(hlavicka(39));
   slowSize=str2double(hlavicka(42));
   Offset=[str2double(hlavicka(45)) str2double(hlavicka(48))];
   ij=[str2double(hlavicka(51)) str2double(hlavicka(54))];
   scanRate=str2double(hlavicka(63));
   dutcycle=str2double(hlavicka(66));
   delay=str2double(hlavicka(69));
   refAmp=str2double(hlavicka(78));
   sineAmp=str2double(hlavicka(81));
   sineFreq=str2double(hlavicka(84));
   sinePhaseShift=str2double(hlavicka(87));
   iGain=str2double(hlavicka(90));
   pGain=str2double(hlavicka(93));
   setpoint=str2double(hlavicka(105));
   dilekx=slowSize/ij(2);
   dileky=fastSize/ij(2);
   X=[dilekx:dilekx:slowSize];
   Y=[dileky:dileky:fastSize];
%     ind=length(filename);
    fid=fopen (filename);
%     HLAVA=textscan(fid,'%s',6);
%     IJa=textscan(fid,'%s',6,'HeaderLines',9);
%     IJ=IJa{1,1};
%     ij=[str2double(IJ{3}),str2double(IJ{6})];

    DAT=textscan(fid,'%n','HeaderLines',34);
    DATa = DAT{1,1,:};
%      A(1:ij(1),1:ij(2))=DATa(((1:ij(2))-1)*ij(1)+(1:ij(2)));
```

```
        for j=1:ij(2)
            for i=1:ij(1)
            HEIGHT(i,j)=DATa((i-1)*ij(2)+j);
            end
        end
%     fclose(fid);
%     surf(X,Y,HEIGHT)
%     shading interp
%     colormap (pink(128))

%% Data Analysis
% vector to matrix
Image = vec2mat(DATa, i);
ImageNorm = Image./max(max(Image));
ImageCrop = imcrop(ImageNorm);
ImageCropNorm = ImageCrop./max(max(ImageCrop));

% image to bw
ImageBW = im2bw(ImageCropNorm);
imshow(ImageBW);

% artefacts and noise reduction
se = strel('disk', 1);
ImageOpen = imopen(ImageBW, se);
ImageClose = imclose(ImageOpen, se);

% segment labelling
ImageSeg = bwlabel(ImageClose);

ShortTemp = zeros(1, max(max(ImageSeg)));
[r, c] = size(ImageSeg);
run = 1;

for D = (length(ShortTemp) - (max(max(ImageSeg))-1)):length(ShortTemp);
        x = [];
        for R = 1:r
            for C= 1:c
                if ImageSeg(R, C) == run
                x = [x, ImageCrop(R, C)];
                end
            end
        end
        run = run+1;
        ShortTemp(D) = max(x)*max(max(Image));
end

longCs = regionprops(ImageSeg, 'MajorAxisLength');
shortCs = regionprops(ImageSeg, 'MinorAxisLength');

longC = cell2mat(struct2cell(longCs))*slowSize/i;
shortC = cell2mat(struct2cell(shortCs))*slowSize/i;

cantilever = shortC - ShortTemp;
LongTemp = longC - cantilever;

Short = [Short, ShortTemp];
Long = [Long, LongTemp];

prompt = 'Load an image?';
loop = input(prompt, 's');
```

```
    if isequal(loop, 'no')
        break
    end
end

AspectRatio = Long./Short;
Mean = mean(AspectRatio);
StDev = std(AspectRatio);

X = ['Nanorods aspect ratio is ', num2str(Mean), ' +- ', num2str(StDev)];
disp(X);
```

APPENDIX C: IMAGE DATA ANALYSIS EXAMPLE

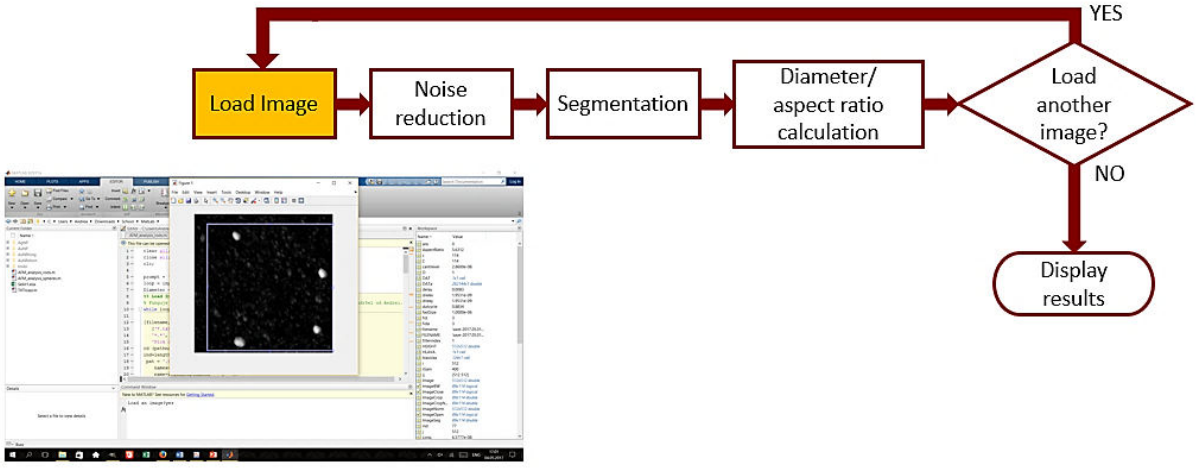

Figure C1: *Image data analysis example. Here, the ASCII image is loaded and displayed in black and white. Black is the background, white are the measured nanoparticles.*

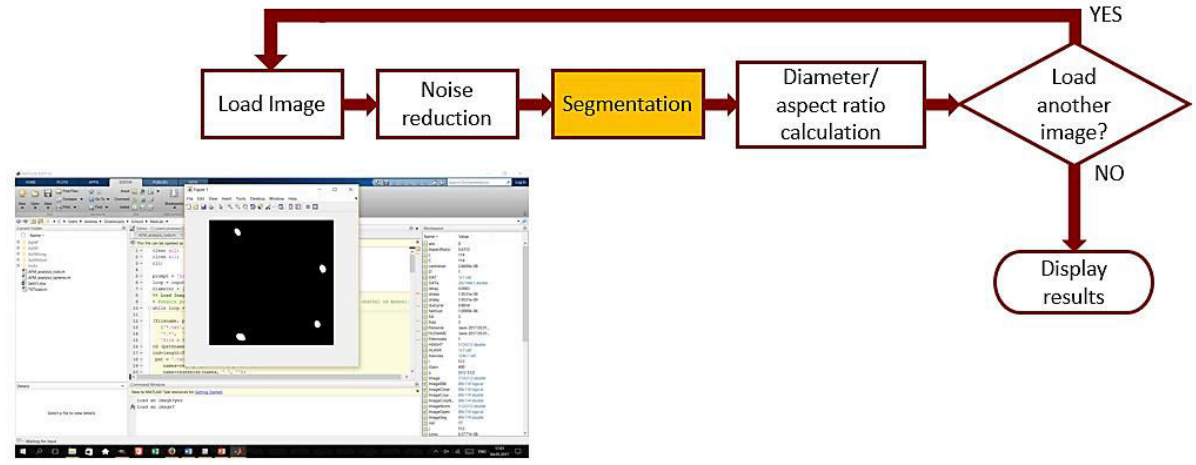

Figure C2: *Image noise reduction and segmentation. Four nanoparticles are later labelled and their diameter is calculated (Figure C3).*

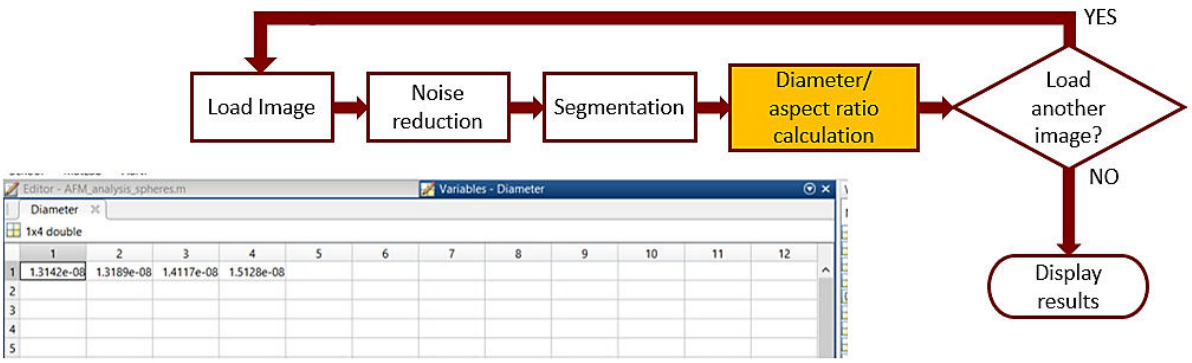

Figure C3: *Calculated diameters of the four nanoparticles in the loaded image. The values are displayed in metres.*

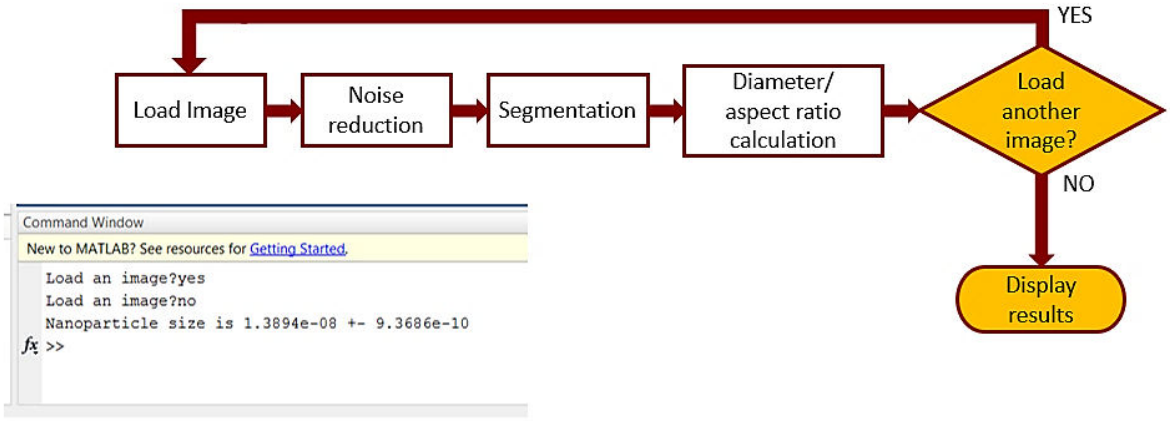

Figure C4: *Required user input in the form of confirming or refusing the loading of another image. If no is the answer, the mean diameter ± standard deviation is displayed. The values are displayed in metres.*

APPENDIX D: ADDITIONAL AFM IMAGES OF SPHERICAL NANOPARTICLES

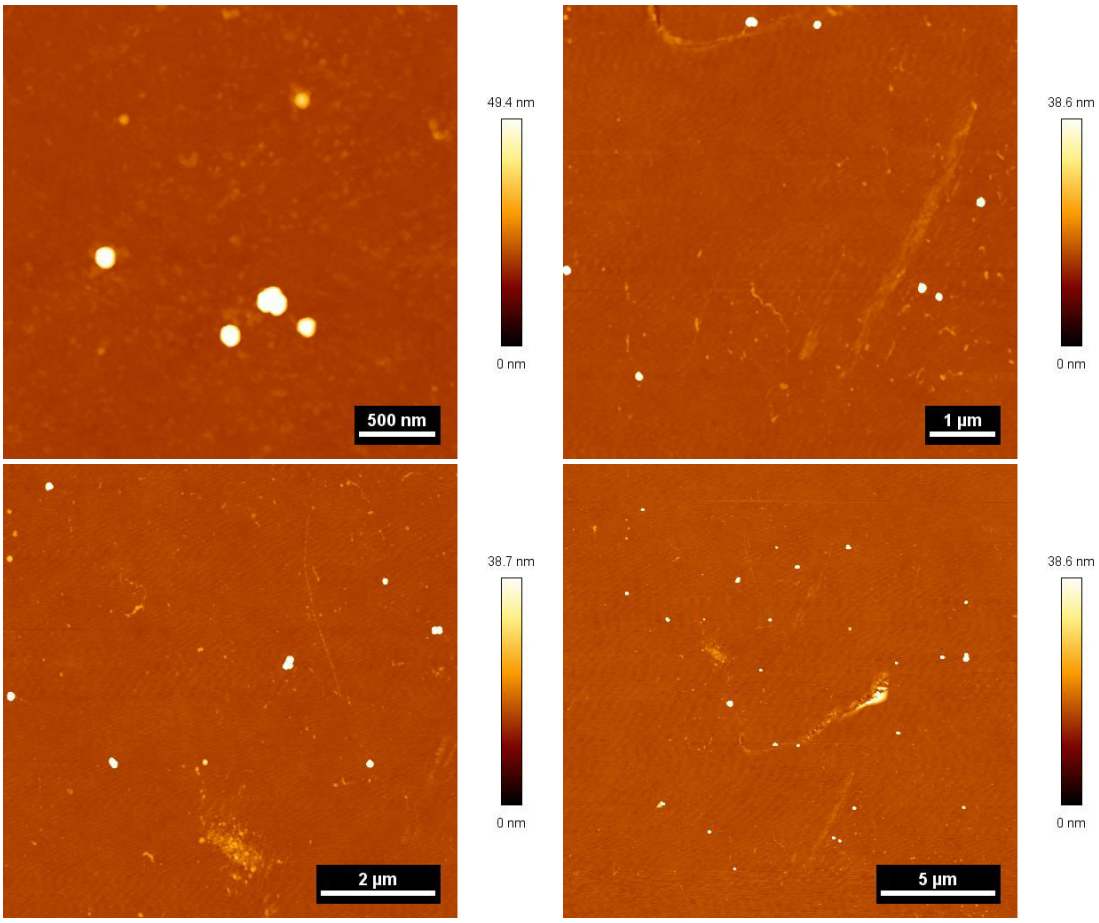

Figure D1: *AFM images of AgNP. Here, different magnifications are presented. Aggregations of few nanoparticles are present in the pictures, this is the reason, why the MATLAB program has a crop option to choose only individual nanoparticles. Each image can be used as input for the image analysis program.*

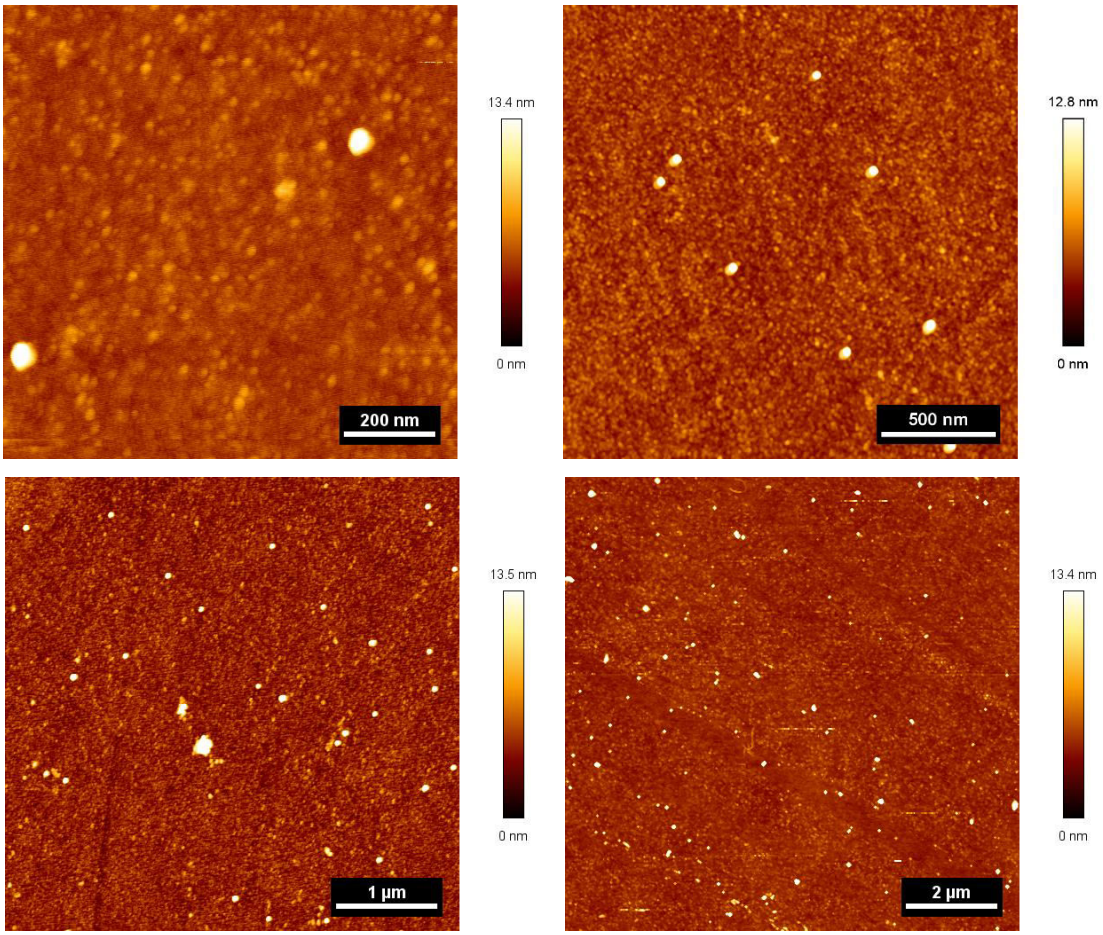

Figure D2: *AFM images of AuNP. Here again, different magnifications are presented. Aggregations of few nanoparticles are present in the pictures, this is the reason, why the MATLAB program has a crop option to choose only individual nanoparticles. Each image can be used as an input for the image analysis program.*

APPENDIX E: ADDITIONAL AFM IMAGES OF NANORODS

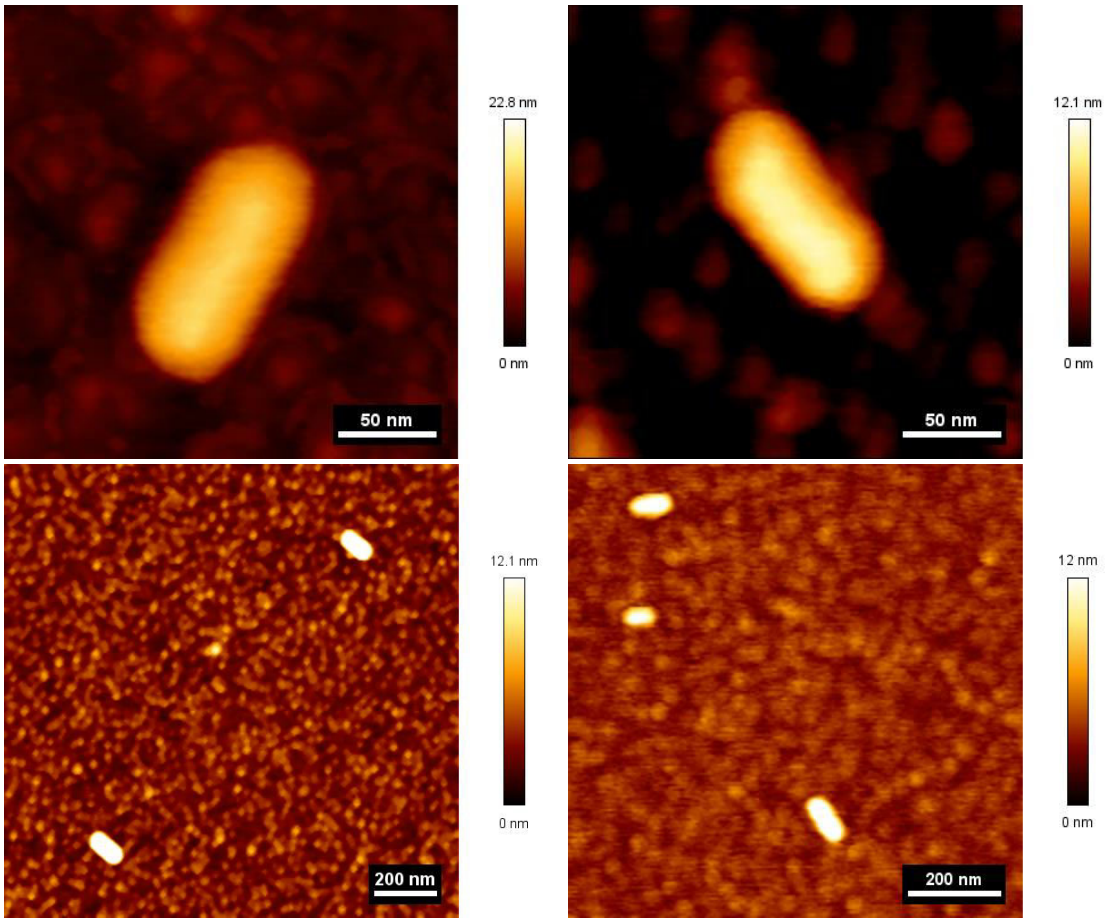

Figure E1: *AFM images of the long AuNR. Two different magnifications for comparison. Both can be used as input for the MATLAB program.*

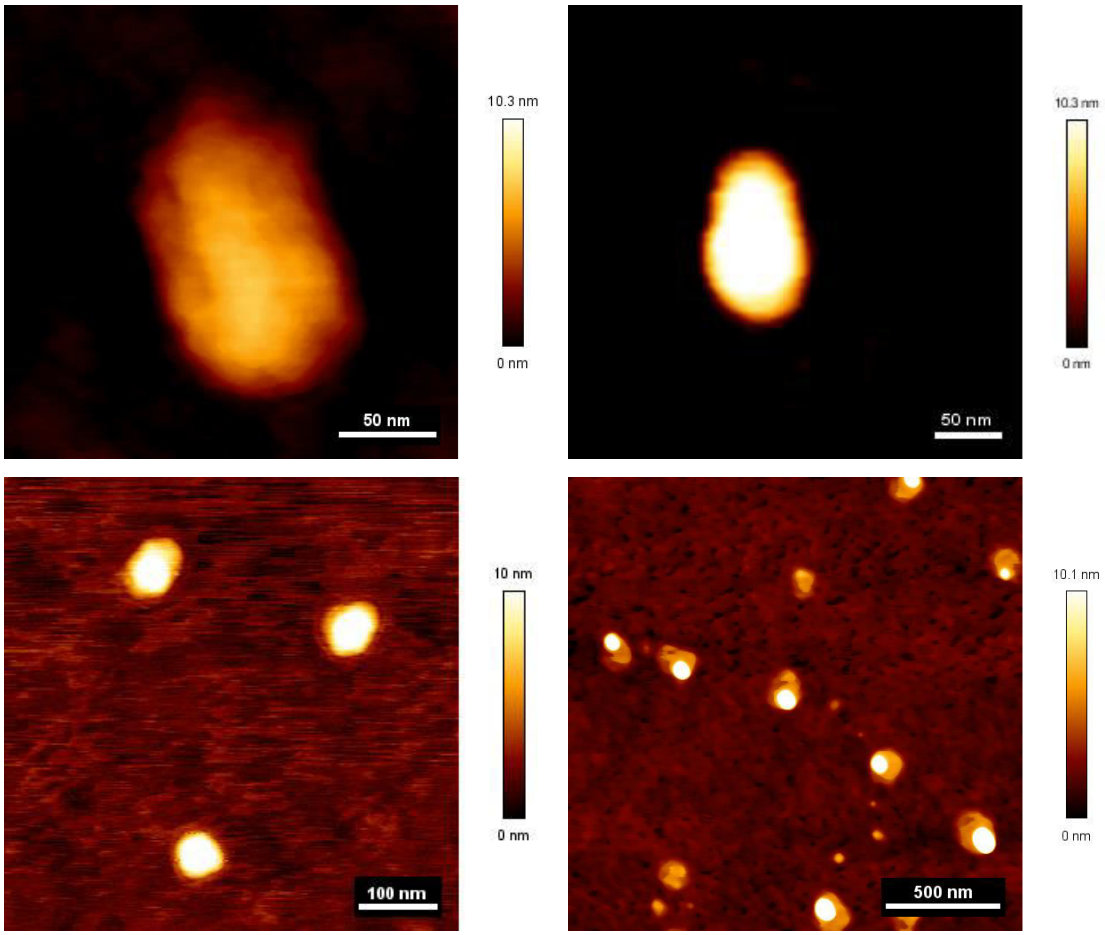

Figure E2: *AFM images of short AuNR. Three different magnifications are shown, each can be used as an input for the image analysis program. Notice the lighter orange places in the last image, these are probably the unwashed CTAB left on the glass surrounding the nanorods (white).*

APPENDIX F: MEASURED ABSORBANCE OF THE NANOPARTICLES

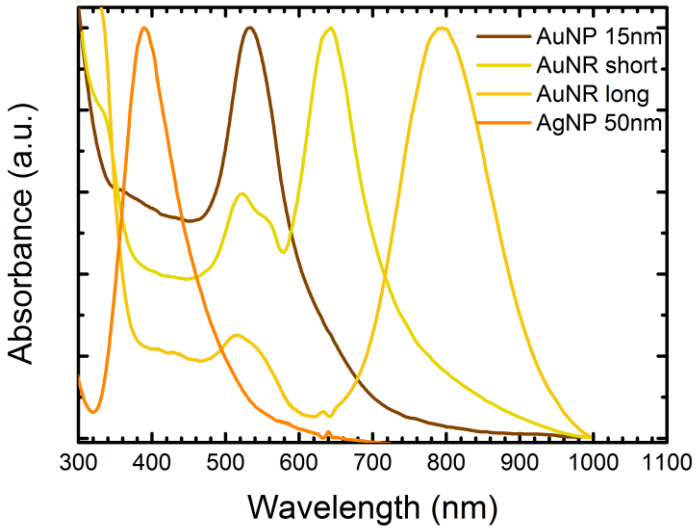

Figure F1: *Measured absorbance of the samples used. It can be seen that short nanorods have an absorbance peak around the wavelength used for the DLS measurements (633 nm).*